Relative sea-level trends in New York City during the past 1500 years

Journal:	*The Holocene*
	Draft
	Paper
	n/a

Kemp, Andrew; Tufts University, Earth and Ocean Science
Hill, Troy; United States Environmental Protection Agency, Atlantic Ecology Division
Vane, Christopher; British Geological Survey,
Cahill, Niamh; University of Massachusetts Amherst, Department of Biostatistics and Epidemiology
Orton, Philip; Stevens Institute of Technology
Talke, Stefan; Portland State University, Department of Civil and Environmental Engineering
Parnell , Andrew ; University College Dublin, Statistics
Sanborn, Kelsey; University of Sydney, School of Geosciences; Tufts University, Earth and Ocean Science
Hartig, Ellen; New York City Department of Parks & Recreation

foraminifera, salt marsh, Bayesian transfer function, carbon isotope, The Bronx, sedimentation

Abstract:

New York City is at risk from 21st century relative sea-level rise because it is likely to experience a regional trend that exceeds the global mean and has high concentrations of low-lying infrastructure and socio economic activity. To provide a long-term context for anticipated future trends, we reconstructed relative sea-level change during the past ~1500 years using a sediment core from a salt marsh at Pelham Bay in The Bronx. Foraminifera and bulk sediment δ13C values were used as sea level indicators, while the history of sediment accumulation was established by radiocarbon dating of plant macrofossils and recognition of pollution and land-use trends of known age in down-core elemental, isotopic, and pollen profiles. The reconstruction was generated within a Bayesian hierarchical model comprised of three modules (calibration, chronology, and process) to accommodate multiple proxies and to provide a unified statistical framework for quantifying uncertainty. We show that relative sea level in New York City rose by ~1.70 m since ~575 CE, of which ~0.38 m occurred after 1850 CE. The rate of relative sea level rise increased markedly between 1852 CE and 1911 CE, which coincides with other reconstructions along the U.S. Atlantic coast. A regional tidal model was used to investigate the possible influence of tidal-range change in Long Island Sound on our reconstruction and we demonstrate that this effect was likely small. However, future tidal-range change could

exacerbate the impacts of RSL rise in co
Sound. The current rate of RSL rise is th
experienced for more than 1500 years a
suggests that projections of 21st centur
realized

RELATIVE SEA-LEVEL TRENDS IN NEW YORK CITY DURING THE PAST 1500 YEARS

Andrew C. Kemp[1*], Troy D. Hill[2], Christopher H. Vane[3], Niamh Cahill[4], Philip M. Orton[5], Stefan A. Talke[6], Andrew C. Parnell[7], Kelsey Sanborn[1,8], and Ellen K. Hartig[9]

1. *Department of Earth and Ocean Science, Tufts University, Medford, MA 02155, USA*
2. *Atlantic Ecology Division, United States Environmental Protection Agency, Narragansett, RI 02882, USA*
3. *British Geological Survey, Center for Environmental Geochemistry, Keyworth, Nottingham, NG12 5GG, UK*
4. *Department of Biostatistics and Epidemiology, University of Massachusetts Amherst, MA, 01003, USA*
5. *Davidson Laboratory, Stevens Institute of Technology, Castle Point on Hudson, Hoboken, NJ 07030, USA*
6. *Department of Civil and Environmental Engineering, Portland State University, Portland, OR 97207, USA*
7. *School of Mathematical Sciences, University College Dublin, Belfield, Dublin 4, Ireland*
8. *Geocoastal Research Group, School of Geosciences, University of Sydney, Sydney, NSW 2006, Australia*
9. *New York City Department of Parks & Recreation, New York, NY 10023, USA*

** Corresponding author; andrew.kemp@tufts.edu; 617-627-0869*

ABSTRACT

New York City is at risk from 21st century relative sea-level rise because it is likely to experience a regional trend that exceeds the global mean and has high concentrations of low-lying infrastructure and socio-economic activity. To provide a long-term context for anticipated future trends, we reconstructed relative sea-level change during the past ~1500 years using a sediment core from a salt marsh at Pelham Bay in The Bronx. Foraminifera and bulk-sediment $\delta^{13}C$ values were used as sea-level indicators, while the history of sediment accumulation was established by radiocarbon dating of plant macrofossils and recognition of pollution and land-use trends of known age in down-core elemental, isotopic, and pollen profiles. The reconstruction was generated within a Bayesian hierarchical model comprised of three modules (calibration, chronology, and process) to accommodate multiple proxies and to provide a unified statistical framework for quantifying uncertainty. We show that relative sea level in New York City rose by ~1.70 m since ~575 CE, of which ~0.38 m occurred after 1850 CE. The rate of relative sea-level rise increased markedly between 1852 CE and 1911 CE, which coincides with other reconstructions along the U.S. Atlantic coast. A regional tidal model was used to investigate the possible influence of tidal-range change in Long Island Sound on our reconstruction and we demonstrate that this effect was likely small. However, future tidal-range change could exacerbate the impacts of RSL rise in communities bordering Long Island Sound. The current rate of RSL rise is the fastest that New York City has experienced for more than 1500 years and its ongoing acceleration suggests that projections of 21st century local relative sea-level rise will be realized.

1. INTRODUCTION

Relative sea-level (RSL) rise is one of the most challenging consequences of climate change and its impact will strongest where (1) local RSL rise exceeds the global average; (2) high concentrations of socio-economic activity and infrastructure are located in low-lying coastal areas; and/or (3) coastal planners and government agencies lack the socio-economic or physical resources that are necessary for effective management and mitigation (e.g., Wong et al., 2014; Nurse et al., 2014). During the 21st century New York City will experience RSL rise greater and faster than the global average (e.g., Horton et al., 2015; Miller et al., 2013; Kopp et al., 2014) because of contributions from ongoing glacio-isostatic adjustment (GIA; e.g., Peltier, 2004; Davis and Mitrovica, 1996), changing patterns of ocean circulation (e.g. Yin et al., 2009; Levermann et al., 2005), and the fingerprint of Antarctic ice melt (e.g., Gomez et al., 2010; Mitrovica et al., 2009). Consequently, RSL rise in New York City may exceed the global average by as much as 32% at the end of this century (e.g., Miller et al., 2013; Kopp et al., 2014; Horton et al., 2015). Furthermore, the intense concentration of population, public and private infrastructure, cultural resources, and economic activity in New York City places it at high risk to RSL rise. Approximately $25.9 bn of property, 93,000 people, seven hospitals, and 183 hazardous waste sites within New York City lie below the Miller et al. (2013) central projection of 0.96 m of local RSL rise by 2100 CE (Surging Seas Project; http://sealevel.climatecentral.org/).

Proxy reconstructions of Common Era (past ~2000 years) RSL trends help frame how anomalous current rates of rise are and provide a paleo constraint for calibrating and testing

models that aim to provide regional-scale projections. On the Atlantic coast of North America these reconstructions are primarily developed from dated sequences of salt-marsh

sediment in which proxies for tidal elevation (termed sea-level indicators) such as foraminifera and plants are preserved (e.g., Kemp et al., 2013a; Gehrels et al., 2005; Donnelly et al., 2004; Kemp et al., 2015). Efforts to reconstruct Common Era RSL usually focus on rural sites because of widespread disturbance and loss of urban saltmarshes. Therefore, existing proxy RSL reconstructions may not reflect trends in the urban centers that are most vulnerable areas to the socio-economic impacts of RSL rise. We address this issue by reconstructing RSL change during the past ~1500 years in New York City using foraminifera and bulk-sediment $\delta^{13}C$ values in a dated core of salt-marsh sediment from Pelham Bay (The Bronx; Long Island Sound). The reconstruction was produced using a Bayesian hierarchical model that formally accommodates two independent sea-level indicators and provides a unified statistical framework for quantifying uncertainty at all stages of the RSL reconstruction including the identification of temporal trends. Due to tidal resonance, changes in the depth of Long Island Sound (e.g. due to RSL rise) cause non-stationary tidal conditions (e.g., Wong, 1990). To assess the possible effect of tidal-range change on our RSL reconstruction, we used archival data (Talke and Jay, 2013) and numerical modeling (Orton et al., 2012) to estimate the influence of increasing depth on tidal range. We conclude that our initial assumption of a constant tidal regime during the past 1500 years is reasonable. In New York City, RSL rose by ~1.70 m since ~575 CE and a continuous acceleration since ~1600 CE means that the current rate of rise is the fastest for more than 1500 years. Our results indicate that recent projections of 21st-century rise requiring accelerated rise are likely to be realized.

2. STUDY SITE

The area of salt marsh in and around New York City decreased rapidly (by ~80%) as the city expanded and coastal wetlands were drained and filled (e.g., Gornitz et al., 2001; Hartig et al., 2002). Along the Hutchinson River in The Bronx, ~0.79 km^2 of salt marsh remains in Pelham Bay Park (Figure 1) and is managed by the New York City Department of Parks & Recreation. The modern salt marsh is experiencing erosion, resulting in a large, unvegetated tidal flat that is characterized by grey, clastic sediment and the presence of marine mollusks. Low salt-marsh zones vegetated by *Spartina alterniflora* are rare at Pelham Bay because of a pronounced (~1 m high), erosional step change in elevation that separates the tidal flat from the high salt-marsh platform. This high salt-marsh zone is vegetated by a peat-forming community of *Spartina patens* and *Distichlis spicata* and is typical of high salt-marsh ecosystems in the northeastern United States that exist between approximately mean high water (MHW) and mean higher high water (MHHW; e.g., van de Plassche, 1991; Redfield, 1972; Johnson and York, 1915). At the boundary between the salt marsh and surrounding, upland forest is a narrow vegetative zone dominated by *Phragmites australis*. This zone is found above the MHHW tidal datum. Peat forming in this environment is typically a black, amorphous organic matrix that hosts the rhizomes of *Phragmites australis* plants (e.g., Niering et al., 1977). Through time these rhizomes are commonly flattened and degraded, resulting in a homogenized peat. The halotype of *Phragmites* found on and around modern salt marshes in the northeastern United States is invasive, although native haloptypes existed prior to European colonization in this region (Saltonstall, 2002). Elsewhere this uppermost zone of marine influence may also be occupied by *Schoeneplectus* spp., *Typha* spp., and/or *Iva fructescens*. We estimated the great diurnal tidal range (mean lower low water, MLLW to MHHW) at the site to be 2.44 m using the VDatum

transformation tool (Yang, 2008), which is comparable to values measured by the National Oceanographic and Atmospheric Administration (NOAA) at the nearby

New Rochelle (2.41 m) and Kings Point (2.38 m) tide gauges (Figure 1). This tidal range is greater than at The Battery (1.54 m) because of the tidal amplification of semi-diurnal tides in the western part of Long Island Sound (e.g., Wong, 1990). We later investigate whether RSL changes may have amplified tidal range over time. Historical tidal-range change was estimated using the Willets Point tide gauge (NOAA gauge 8516990; 1931-2000) and one year of hourly tide-gauge data measured in 1892 by the U.S. Coast and Geodetic Survey at Willets Point (Talke and Jay, 2013). Within New York City, tide gauges at The Battery, Willets Point, Kings Point and New Rochelle (Figure 1) measured the same RSL variability during the 20th century (Figure 2), indicating that annual to multi decadal-scale sea-level trends are geographically consistent between New York

Harbor and Long Island Sound.

3. METHODS

3.1 Core collection and leveling

The sediment beneath the Pelham Bay salt marsh was described from hand-driven cores collected along two transects (Figure 1C, D). Core PBA-4 was selected for detailed analysis because it included the thickest accumulation of peat and was therefore anticipated to provide the longest RSL record and adequate material for radiocarbon dating. We consider PBA-4 to be representative of the stratigraphy underlying the site and its paleoenvironmental history, including RSL changes. The core was collected in overlapping 50-cm long sections using a

Russian core to avoid compaction or contamination during sampling. Each core segment was

placed into a rigid plastic sleeve, labeled, wrapped in plastic, and stored in refrigerated conditions prior to laboratory analysis.

Core top elevations were measured by leveling them to a local benchmark using a TopCon GPT-3200NW total station (vertical accuracy of 2 mm + 2 ppm). The benchmark elevation was established relative to the North American Vertical Datum of 1988 (NAVD88) using real time kinematic satellite navigation measurements by a professional surveyor. We deployed an automatic water-level logger (Solinst® Levelogger Edge) at Pelham Bay (Figure 1) and also leveled it to the benchmark. The logger measured water levels at six minute intervals (the same as those made at NOAA tide gauges) for 252 tidal cycles between 25 July and 12 December 2012. After correcting the water-level measurements for variations in atmospheric pressure measured simultaneously by a second logger, high tides and low tides at Pelham Bay were isolated from the water-level logger dataset. To account for the relatively short duration of water-level measurements at Pelham Bay, we correlated local high tides with those recorded by the nearby (~8 km) NOAA-operated tide gauge at Kings Point (station number 8516945). The relationship between Pelham Bay and Kings Point (R^2 = 0.95; Figure 2B) was used to generate a dataset of high tides at Pelham Bay from when the Kings Point tide gauge became operational (1999) to the year of core collection (2012). Tidal datums at Pelham Bay were estimated from this dataset.

3.2 Sea-level indicators

Studies of modern salt-marsh (and mangrove swamp) foraminifera at locations around the world repeatedly demonstrated that they have a systematic, quantifiable and predictable relationship to

tidal elevation making them sea-level indicators (e.g., Scott and Medioli, 1978; Edwards and Wright, 2015; Gehrels, 2000; Horton and Edwards, 2006). The use of foraminifera as sea-level indicators is grounded in reasoning by analogy, where assemblages preserved in cores of salt-marsh sediment are interpreted by comparison to modern assemblages. This approach relies on the availability of an appropriate modern training set comprised of paired observations of tidal elevation and species abundances. Since the composition of foraminiferal assemblages varies spatially in response to secondary environmental variables such as salinity and climate, it is necessary to use a suitable local- or regional-scale training set (Horton and Edwards, 2005; Kemp et al., 2013b). Objective interpretations can be made using a transfer function to formalize the relationship between foraminifera and tidal elevation using empirical observations (e.g., Kemp and Telford, 2015). A variety of specific numerical methods are available to construct transfer functions (e.g., Juggins and Birks, 2012). This approach can resolve late Holocene RSL changes on the order of 1-10s of centimeters where suitable sequences of salt-marsh sediment exist (see, for example, reviews in Barlow et al., 2013; Gehrels and Woodworth, 2012). The surface distribution of dead, salt-marsh foraminifera at 12 sites on the north coast of Long Island Sound (including Pelham Bay) was described by Kemp et al. (2015) based on original and existing data (Edwards et al., 2004; Gehrels and van de Plassche, 1999; Wright et al., 2011). This regional-scale dataset of 254 samples provided the modern training set necessary to estimate paleomarsh elevation (PME), defined as the tidal elevation at which assemblages preserved in PBA-4 were originally deposited. Due to differences in the tidal range among sites, sample elevations in the modern training set were expressed as a standardized water level index (SWLI; e.g., Horton and Edwards, 2006), where a value of 100 corresponds to local MHHW and a value of 0 corresponds to local mean tide level (MTL).

Foraminifera were enumerated from 1-cm thick samples of core PBA-4 that were spaced every 2 cm to a depth of 1.60 m. Each sediment sample was washed over 63 µm and 500 µm sieves to separate and retain the foraminifera-bearing fraction. A minimum of 100 specimens suspended in water were counted under a binocular microscope. If fewer than 100 tests were present, the entire sample was counted. Species were identified by comparison to type slides of modern specimens. To ensure consistency with the modern training set, *Trochammina inflata* and *Siphotrochammina lobata* were combined into a single group prior to analysis (Wright et al., 2011). Down-core counts of foraminifera are presented in the supporting appendix.

The dominant source of organic material deposited on salt marshes in the northeastern U.S. is *in-situ* above and below ground biomass from plants (e.g., Chmura and Aharon, 1995; Middleburg et al., 1997). The ratio of stable carbon isotopes ($\delta^{13}C$) in bulk sediment therefore reflects the dominant vegetation community at the time of deposition and can be used to verify or constrain estimates of PME made by transfer functions because plant communities on salt marshes are also sea-level indicators (e.g., Johnson et al., 2007; Kemp et al., 2012b; Waller, 2015; Shennan, 1986). On the U.S. mid-Atlantic and northeast coasts the MHHW tidal datum is the boundary between communities of salt-marsh plants dominated by C_3 (e.g., *Phragmites australis*) and C_4 (e.g., *Spartina patens* and *Distichlis spicata*) species (e.g., Kemp et al., 2012b; Middleburg et al., 1997). The difference in carbon isotope signatures between C_3 and C_4 plants is considerably larger than within-group variability and is therefore easily detectable (e.g., Peterson et al., 1985; Lamb et al., 2006; Tanner et al., 2007; Nydick et al., 1995). Consequently, an empirical dataset from a site in New Jersey with the same zonation of salt-marsh plants as

Pelham Bay demonstrated that bulk-sediment samples that formed below MHHW yielded $\delta^{13}C$ measurements that are less depleted than -18.9

‰ relative to the Pee Dee Belemnite (PDB) standard, while samples that formed above MHHW have $\delta^{13}C$ measurements that are more depleted than -22.0 % (Kemp et al., 2012b). We used these threshold values to identify intervals in core PBA-4 that were likely to have accumulated above or below the MHHW tidal datum following Cahill et al. (2016). We anticipate that local variability in threshold values is considerably smaller than the difference between bulk-sediment values from environments dominated by C_3 and C_4 plants (compare for example Tanner et al., 2007; Johnson et al., 2007; Middleburg et al., 1997; Kemp et al., 2012b). Rather than apply threshold values to individual samples in isolation, we divided the core into sections characterized by persistent $\delta^{13}C$ values.

This conservative approach further serves to dampen any potential influence of local-scale variability in threshold values. We measured $\delta^{13}C$ and total organic content (TOC) on undifferentiated (bulk), 1-cm thick sediment samples from core PBA-4 using standard methods at the Yale University Analytical and Stable Isotope Center (tabulated data are provided in the supporting appendix).

3.3 Age-depth markers

Discrete depths in PBA-4 were assigned ages using either radiocarbon dating of macrofossils (pre-1600 CE) or recognition of anthropogenic markers of known age (post-1600 CE). The macrofossils used for radiocarbon dating were isolated from the sediment matrix, washed with deionized water, and identified using a reference collection of modern salt-marsh plants and illustrated texts (e.g., Niering et al., 1977). Each sample was further cleaned under a binocular

microscope to remove ingrowing material and adhered sediment before being dried in an oven at ~40°C. The dry samples

were submitted to the National Ocean Sciences Accelerator Mass Spectrometry (NOSAMS) laboratory for radiocarbon dating where they underwent standard acid-base-acid pretreatment. Sample $\delta^{13}C$ was measured on an aliquot of CO_2 collected during combustion. The radiocarbon ages reported by NOSAMS are presented in Table 1.

A plateau in the radiocarbon calibration curve results in multiple calibrated ages and large chronological uncertainty for samples that formed since ~1600 CE (Stuiver and Pearson, 1993). To address this limitation, we dated the more recently-deposited portion of PBA-4 by recognizing pollution and land-use trends of known age in down core profiles of elemental and isotopic abundance and pollen. We measured the concentrations of a suite of elements and lead isotopes on 1-cm thick, bulk-sediment samples using the methods and instruments described in Vane et al. (2011). The activity of ^{137}Cs was measured by gamma spectroscopy at Yale University using standard methods (e.g., Anisfeld et al., 1999). Samples for pollen analysis were prepared following the method outlined in Traverse (2007) and a minimum of 300 pollen grains were counted from each sample. Tabulated elemental measurements, isotopic measurements and pollen counts are presented in the supporting appendix.

Down core changes in elemental and isotopic concentrations were matched to local and regional pollution patterns of known age to estimate the age of specific depths in PBA-4. We assumed that industrial emissions were transported from their source by constant prevailing winds and without further isotopic fractionation (e.g., Gobeil et al., 2013; Lima et al., 2005; Chillrud et al.,

1999; Kemp et al., 2012a). Since the core site is located in a high salt-marsh environment, our interpretation of elemental and isotopic profile

s assumes that pollution was delivered through direct deposition from the atmosphere and/or supplied by tidal water that was representative of regional pollution trends (e.g., Marshall, 2015; Varekamp, 1991; Cochran et al., 1998).

However, this assumption may be invalidated in the case of localized pollution events such as spills. Since emissions/discharge per unit of production likely changed through time, recognition of chronohorizons was based on trends rather than absolute values. All age markers were assigned an age and depth uncertainty to reflect the lag time between emission/discharge and deposition and the range of possible depths in the core that correspond to an individual trend. This approach yielded a suite of age-depth estimates (with individual vertical and temporal uncertainties), all of which were retained in the age-depth model (section 3.4).

3.4 The Bayesian hierarchical model

We reconstructed RSL using the Bayesian hierarchical model of Cahill et al. (2016) . The model is comprised of three, linked modules that were implemented separately, but share a unified numerical framework to provide consistency and appropriate propagation of uncertainty.

(1) In the calibration module, we developed a Bayesian transfer function (B-TF) to formalize the observed relationship between modern assemblages of foraminifera (expressed as raw counts) and tidal elevation (expressed as a SWLI) using the regional dataset of 254 samples from 12 sites around Long Island Sound. The B-TF of Cahill et al. (2016) assumes a multinomial model for foraminiferal assemblages, and uses a set of penalized spline smoothing functions (Lang and Brezger, 2004) to describe the non-linear response

o f i n d i v i d u a l f o r a m i n i f e r a l s

pecies to tidal elevation. The parameters that describe each species response curve were estimated from the modern training set. Application of the B-TF to assemblages of foraminifera preserved in PBA-4 generated posterior estimates of PME with a 2σ, sample-specific uncertainty. When applied to core samples, the B-TF requires a prior specification for PME, which can be informed by the modern training data. In this study, the organic nature of the core sediment and presence of foraminifera indicated that all samples accumulated above MTL (SWLI = 0), but below the highest occurrence of foraminifera in the regional modern training set (SWLI = 154, rounded up to 155). Hence, the prior favors values between 0-155 SWLI.

Within the B-TF, measurements of $\delta^{13}C$ provided an additional, formalized constraint on PME. Intervals in the core where $\delta^{13}C$ values were more depleted than -22.0 ‰ were assumed to form at elevations between MHHW and the highest occurrence of foraminifera in the modern training set (SWLI = 100-155). For intervals where $\delta^{13}C$ values were less depleted than -18.9 ‰, we assumed that samples formed between MTL and MHHW (SWLI = 0-100). These additional constraints were not treated deterministically, but rather serve to reduce or increase the likelihood that PME lies above or below the thresholds. Parts of the core where bulk-sediment samples predominately had intermediate (-22.0 ‰ to -18.9 ‰), or variable, $\delta^{13}C$ values were not subject to any additional constraint (SWLI = 0-155). The height of RSL (rounded to the nearest centimeter) was reconstructed by subtracting the PME estimated by the B-TF from the measured altitude of the sample (depth in core, where the core top was leveled to local tidal datums) under an initial assumption that the tidal regime at Pelham Bay was

unchanged for the period under investigation. This ass
effect of tidal-range change is explored.

Performance of the B-TF was assessed using a cross valida
modern training set was divided into ten, randomly-drawn
folds). Each fold was removed from the modern training s
used to predict the elevations of the excluded samples with
repeated until every sample in the modern training set had

The ecological plausibility of the PME reconstructions was
(Bray-Curtis) dissimilarity between each core sample and i
training set. If the closest analogue for a core sample exce
dissimilarity measured among all possible sample pairings
classified as lacking an appropriate modern analogue and v

the resulting probability distributions. Chronohorizons identified from pollution and pollen trends were assigned a uniform probability within their stated age uncertainty. The Bchron model does not impose a pattern of sedimentation (linear or otherwise), but rather generated a large suite of equi-probable chronologies for PBA-4 using Markov Chain Monte Carlo simulation. From these possible chronologies, Bchron estimated the age of each 1-cm thick layer. We present and discuss the mean and 95% credible interval; all age estimates are rounded to the nearest whole year. Each sample with a valid PME reconstruction was an assigned the corresponding age (with uncertainty) from the Bchron age-depth model. In addition, we used the suite of possible chronologies generated by Bchron to provide a probabilistic history of sediment accumulation, in which mean annual sedimentation is estimated with uncertainty (reported as the 90% credible interval, expressed in mm/yr and rounded to one decimal place).

(3) The process module was an Errors-In-Variables Integrated Gaussian Process (EIV-IGP) model for estimating rates of sea-level change through time with uncertainty (Cahill et al., 2015a). This model accounts for the unique combination of age and vertical uncertainties (and their probability distributions) in each data point and their uneven spacing through time to estimate a continuous time series of RSL and rates of RSL change. We combined the new, proxy-based RSL reconstruction from Pelham Bay with decadal average tide-gauge measurements from The Battery to produce a RSL history for New York City. The EIV-IGP model was applied to this dataset. To complement results from the EIV-IGP model, we also used change-point analysis (Carlin et al., 1992; Cahill et al., 2015b) to objectively identify distinctive phases of RSL change in New York City. This approach models the RSL

reconstruction as sequential linear trends that are joined to one another at change points. The number and timing of change points is estimated quantitatively and with uncertainty from the RSL data. Deviance information criterion (Spiegelhalter et al., 2002) combined with parameter convergence checks were used to detect the appropriate number of change points.

4. RESULTS

4.1 Performance of the Bayesian transfer function

We judged the performance of the B-TF using cross validation of the modern training set (section 3.4). For 221 of the 254 samples, the elevation measured at the time of sample collection falls within the 95% credible interval of the elevation predicted by the B-TF (Figure 3A). The average difference between actual and mean predicted elevation was 5 SWLI (approximately 0.06 m at Pelham Bay). No visible structure (trends between residual values and actual elevation) was observed in these residuals, indicating that the B-TF did not systematically over or under predict PME and can accurately reconstruct PME across the sampled range of tidal elevations (Figure 3B).

4.2 Sea-level indicators in Pelham Bay core 4

Core PBA-4 comprised four distinct units of sediment. The basal unit is blue-brown sand and silt that we consider to be an incompressible, pre-Holocene substrate of glacial origin. At salt marshes along the northeastern U.S. Atlantic coast, the boundary between glacial substrate and overlying organic units almost always represents a hiatus of non-deposition and/or erosion spanning several thousand years (e.g., Donnelly, 2006; Nydick et al., 1995; van de Plassche, 1991; Gehrels, 1994; Donnelly and Bertness, 2001). At Pelham Bay the pre-Holocene substrate

is overlain by a unit of brown, organic silt with measured TOC content of <6% (Figure 4A). At depths from approximately 160 cm to 55 cm, the sediment was comprised of relatively dry black peat. In the lower part of this third unit only the remains of *Phragmites australis* were identified, while in the upper part the remains of *Spartina patens* and *Distichlis spicata* were increasingly present. The average TOC content of this unit was 34% and reached a maximum of 45.7%. The upper 55 cm of the core was characterized by a brown, high salt-marsh peat with abundant remains of *Spartina patens* and *Distichlis spicata*. The average TOC content of this unit was 23.6%. The boundary between these contrasting units of peat was not erosive and did not indicate a hiatus in sedimentation at any location where we described cores. The transition seen in plant macrofossils from *Phragmites australis* to *Spartina patens* and *Distichlis spicata* and reduced TOC values indicates a long-term RSL transgression at Pelham Bay. Measured TOC values are typical of modern and late Holocene high salt-marsh environments in the study region (e.g., Bricker-Urso et al., 1989; Nydick et al., 1995; Morris et al., 2016).

In PBA-4, foraminifera were absent at depths below 160 cm in the basal sand and silt and in the lowermost part of the brown, organic silt unit (Figure 4B). Between 160 cm and 40 cm the dominant species of foraminifera was *Jadammina macrescens* (average 81.7%). At depths above 40 cm, there was an increase in the abundance of *Trochammina inflata* and *Siphotrochammina lobata* (average 40.8% when combined) with a corresponding decline in the abundance of *Jadammina macrescens*. The average abundance of *Tiphotrocha comprimata* was 18.7% at depths above 64 cm compared to 4.4% below. These species of foraminifera are typical of peat-forming, high salt-marsh environments in the northeastern United States (e.g., Kemp et al., 2015; Gehrels, 1994; Wright et al., 2011) and maritime Canada (e.g., Scott and Medioli, 1980;

Scott et al., 1981; Wright et al., 2011). Six samples (out of 85) in the core yielded counts of fewer than 50 individuals (at 100 cm, 102 cm,

154 cm, 156 cm, 158 cm and 160 cm) and were excluded from further analysis. Four of the remaining samples had counts from 66 to 99 individual foraminifera.

Bulk-sediment $\delta^{13}C$ values below 130 cm in PBA-4 were typical of C_3 plants (average -27.1 ‰) and were more depleted than the threshold (-22.0 ‰) used to identify sediment that accumulated above MHHW (Figure 4C). The interval between 130 cm and 67 cm was characterized by variable $\delta^{13}C$ values that ranged from -23.3 ‰ to -15.1 ‰. In the uppermost 63 cm of PBA-4, the average $\delta^{13}C$ value was -15.7 ‰ and all samples were less depleted than the threshold of -18.9 ‰ used to identify samples that accumulated below MHHW, with the exception of two samples (at 1 cm and 4 cm) with intermediate values between those typical of C_3 and C_4 vegetation.

4.3 Application of a Bayesian transfer function to reconstruct paleomarsh elevation

Application of the B-TF to assemblages of foraminifera enumerated from PBA-4 produced reconstructions of PME with a 2σ, sample-specific uncertainty (Figure 4D). PME estimates were constrained using $\delta^{13}C$ values to identify intervals where there was high likelihood that the sediment accumulated between MHHW and the highest occurrence of foraminifera (100-155 SWLI; below 127 cm in PBA-4), or between MTL and MHHW (0-100 SWLI; 7-67 cm in PBA-4). The measured $\delta^{13}C$ values between 126 cm and 68 cm and above 6 cm did not provide any additional information to constrain the PME reconstruction. Below 127 cm the average reconstructed PME lay slightly above MHHW (115 SWLI) and had an average, 2σ uncertainty of

± 15.5 SWLI. From 126 cm to 68 cm,

reconstructed PME was more variable (means from 94.9 to 143.0 SWLI) and had larger average uncertainties (± 22.5 SWLI) than the underlying part of the core because intermediate $\delta^{13}C$ values did not provide an additional constraint on the reconstruction. Samples from 66 cm to 6 cm yielded average PME reconstructions of 89.7 SWLI with an average uncertainty of ± 9.0 SWLI, although the uncertainty for some samples was as low as ± 5.5 SWLI.

The ecological plausibility of reconstructed PME was judged by measuring dissimilarity between the assemblage of foraminifera in each core sample and its closest modern analog (section 3.4; Figure 4E). The closest modern analogs for the 79 samples in PBA-4 with counts exceeding 50 individuals were drawn from ten of the 12 sites in the regional-scale modern training set. Four core samples lacked a modern analog. The samples at 62 cm, 72 cm, and 76 cm had unusually high abundances of *Miliammina petila* (11-21%) compared to the modern training set in which this species had a maximum abundance of 6.3%. A similar study in New Jersey also recognized that relatively high abundances of *Miliammina petila* in core material resulted in no modern analogue outcomes (Kemp et al., 2013a). Finding the modern analogue to this assemblage would therefore be useful to support efforts to reconstruct RSL. The sample at 155 cm included 19% *Tiphotrocha comprimata* and 78% *Jadammina macrescens*. It likely lacked a modern analogue because the high concentration of samples close to MHHW (Figure 3) coupled with the low-diversity of foraminiferal assemblages in the modern training set resulted in a high degree of similarity among modern samples and consequently a low value for the 20th percentile dissimilarity threshold. This was highlighted as a possible limitation of this approach for assessing ecological plausibility by Kemp and Telford (2015).

4.4 Core chronology and sedimentation rates

Regional-scale pollution markers were recognized in down core concentrations of lead, copper, and vanadium, the ratio of stable lead isotopes (^{206}Pb:^{207}Pb), and measured ^{137}Cs activity (Figure 5A). The late 19th century onset of regional-scale lead pollution was obscured in PBA-4 by a pronounced peak in concentration at 50-60 cm that we interpreted as a local event of unknown provenance, since it was not present at locations in New Jersey (Kemp et al., 2012a), Connecticut (Kemp et al., 2015; Varekamp, 1991; Varekamp et al., 2005), or elsewhere in New York City (Chillrud et al., 1999). Based on its estimated timing (~1730 CE to ~1830 CE) possible sources include tanneries, which were common in New York City during this interval (Burrows and Wallace, 1999) and frequently produce waste that includes high concentrations of metals including lead (e.g., Haroun et al., 2007; Walraven et al., 1997). A small peak in lead concentration at ~39 cm was interpreted as the expansion of production and consumption following World War I, while a decline at ~27 cm corresponds to reduced industrial production (and consequently pollution) during the Great Depression. The peak in lead concentration at ~11 cm marks the introduction of the Clean Air Act and was assigned an age of 1974 CE. National production records indicate that the onset of copper pollution occurred at ~1900 CE, which is recorded in PBA-4 at ~33 cm. Maximum copper concentration occurred at depths between approximately 10 cm and 20 cm, which correspond to peaks in national production and consumption at ~1970 CE. Sedimentary records from nearby salt marshes in Connecticut confirm the presence and timing of these features in the study region (Varekamp et al., 2005; Varekamp, 1991). A peak in Vanadium concentration at ~11 cm was assigned an age of ~1970

ional-scale decline in fuel oil use (Chillrud et al., 1999; Kamenov et al., 2009).

The changing ratio of stable lead isotopes in PBA-4 identified four chronohorizons. The increased ^{206}Pb:^{207}Pb ratio at ~50 cm reflects the onset of lead production in the Upper Mississippi Valley at ~1827 CE (Doe and Delevaux, 1972; Heyl et al., 1966). The emissions from this early industrial activity were carried to the Atlantic coast of North America by prevailing winds (e.g. Graney et al., 1995; Lima et al., 2005; Gobeil et al., 2013; Kelly et al., 2009) and caused a change in stable lead isotope ratios because of the unusual composition of the galena ore used at that time (Heyl et al., 1966; Heyl et al., 1974) coupled with low background concentrations of lead. The peak at ~40 cm in PBA-4 reflects the time (~1857 CE) when the Upper Mississippi Valley made its highest proportional contribution to national lead production. A decline in the ^{206}Pb:^{207}Pb ratio to a minimum at ~15 cm was caused by the introduction of leaded gasoline (after 1923 CE; Facchetti, 1989) with a low ^{206}Pb:^{207}Pb signature of ~1.165 (Hurst, 2000). The rise in ^{206}Pb:^{207}Pb ratio to a peak at ~5 cm (~1980 CE) was caused by the increasing use of lead ore from Missouri in gasoline and the phasing out of all leaded gasoline (by 1993 CE U.S. lead emissions from gasoline were 1% of those in 1970 CE; Bollhöfer and Rosman, 2001). The first detectable horizon of ^{137}Cs activity (~11 cm) was assigned an age of 1954 CE, corresponding to the start of widespread, above ground testing of nuclear weapons which peaked in 1963 CE (~7 cm in PBA-4).

The location of Pelham Bay within New York City results in the presence of local-scale pollution markers. According to Walsh et al. (2001), the use of municipal refuse incinerators

throughout New York City generated air-borne pollution that was subsequently deposited directly from the atmosphere. The discharge from these incinerators peaked at ~1937 CE and the emitted ash included anomalously high concentrations of arsenic, cadmium, selenium, tin and nickel compared to the crust. In PBA-4, we identified a peak in these elements at ~21 cm that likely corresponds to the incineration of refuse (Figure 5B).

Prior to industrialization, anthropogenic modification of the landscape in the northeastern United States consisted of land clearance to provide raw materials for building and space for grazing and agriculture (e.g., Brugam, 1978; McAndrews, 1988; Fuller et al., 1998). This activity increased the amount of pollen from weeds such as *Ambrosia* and a corresponding decline in native forest species. In addition, deforestation likely mobilized sediment that was eroded from upland regions and transported to the coast. According to Kirwan et al. (2011), this process delivered large quantities of titanium and potassium to coastal marshes. In PBA-4, we identified a land clearance horizon at ~60 cm from the rise of *Ambrosia* and *Pinus* pollen, the decline of *Carya* (hickory) pollen, and increased concentrations of titanium and potassium (Figure 5C). The rise of *Plantago* and *Amaranthaceae* also indicates extensive land clearance from this time onward. This horizon was assigned an age of 1680 CE ± 25 years based on the history of settlement in the study region (e.g., Pederson et al., 2005; Burrows and Wallace, 1999).

All radiocarbon dates and age markers in PBA-4 were combined and used as the input to the Bchron age-depth model (section 3.4; Figure 5). The average age uncertainty (95% credible interval) for a 1-cm thick interval of PBA-4 was ± 50 years and ranged from ± 115 years at 1.14 m to ± 3 years at 0.08-0.10 m. Prior to ~1800 CE, the mean annual accumulation rate in PBA-4

was ~0.5 mm/yr, with an average

90% credible interval of 0.2 to 2.3 mm/yr (Figure 6A). There was short-lived pulse of sedimentation at ~1820-1845 CE (up to 2.0 mm/yr). From ~1890 CE onwards, mean annual sedimentation rates increased sharply to achieve an average 20th century rate of 3.0 mm/yr (90% credible interval of 0.8-13.0 mm/yr). To provide a direct comparison with Pelham Bay we reanalyzed sedimentation rates from representative salt marshes in Connecticut (East River Marsh; Kemp et al., 2015) and southern New Jersey (Cape May Courthouse; Kemp et al., 2013a: ; Figure 6B). In Connecticut, the pre-1800 CE sedimentation rate was ~0.6 mm/yr. A sediment shortly after 1850 CE was followed by an average 20th century rate of 1.9 mm/yr (90% credible interval of 0.5-11.2 mm/yr). In New Jersey, the mean annual, pre-1800 CE sedimentation rate was 1.0 mm/yr (90% credible interval of 0.3-4.7 mm/yr). A pulse of sedimentation occurred at ~1820-1870 CE and the average rate of sedimentation during the 20th century was 2.6 mm/yr (90% credible interval of 0.8-10.7 mm/yr; Figure 6B). This temporal evolution is typical of salt marshes along the Atlantic coast of North America (e.g., Kemp et al., 2015; Varekamp et al., 1992; van de Plassche et al., 1998; Donnelly et al., 2004; Nydick et al., 1995; Engelhart et al., 2009; Kemp et al., 2014; Kemp et al., 2011; Kemp et al., 2013a) where sedimentation rates on multi-decadal and longer timescales are closely linked to the rate of RSL rise (e.g., Morris et al., 2002; Kirwan and Murray, 2007; Kirwan and Murray, 2008). The long-lived background rates of sedimentation reflect RSL rise driven primarily by spatially-variable GIA, while recent rates of rise occur because of the salt marsh response to accelerated RSL rise beginning in the late 19th century. For example, at salt marshes on the Connecticut and New York coasts of Long Island Sound (including a different core from Pelham Bay), Hill and Anisfeld (2015) reported that regional, decadal-scale sediment accretion rates increased from ~1.0 mm/yr at 1900 CE to current rates of ~3.6 mm/yr in response to accelerating

RSL rise. Similar annual-to-decadal rates of salt-marsh sediment accretion in the 20th century are also reported by other studies 8

conducted in this region (e.g., Harrison and Bloom, 1977; Roman et al., 1997; McCaffery and Thomson, 1980). We conclude that the history of sediment accumulation estimated for PBA-4 is typical of salt marshes in Long Island Sound and that our RSL reconstruction is not a reflection of local and anomalous sediment accumulation arising from its location in an urban salt marsh.

4.5 Relative sea-level change at Pelham Bay

The new proxy-based RSL reconstruction from Pelham Bay is comprised of 75 data points with an average, 2σ vertical uncertainty of ± 0.19 m and an average 2σ chronological uncertainty of ± 50 years (Figure 7A; tabulated in supporting appendix). It shows that RSL rose continuously from approximately -1.7 m at 575 CE to 0 m at present. Change point analysis divided the RSL record into three linear phases separated by significant changes in rate at 1015-1238 CE (secondary change) and 1852-1911 CE (primary change; Figure 7B). The EIV-IGP model described the continuous evolution of RSL change and estimated that the rate of RSL rise was ~0.5 mm/yr at 600-1000 CE, increased to a peak of 1.52 mm/yr (1.19-1.85 mm/yr; 95% credible interval) at ~1400 CE, and subsequently slowed to 1.37 mm/yr (1.07-1.67 mm/yr; 95% credible interval) at ~1630 CE. Since this minimum the rate of RSL rise increased continuously to attain a current rate of 2.98 mm/yr (2.13-3.84 mm/yr; 95% credible interval), which is the fastest rate in the last ~1500 years and in agreement with the average rate measured in New York Harbor from 1900 CE to 2012 CE (2.7-3.3 mm/yr; Kopp, 2013).

5. DISCUSSION

5.1 Late Holocene relative sea-level trends in New York City

The Battery tide gauge (among the longest and most complete records in the world) measured an average, linear RSL rise of 2.83 mm/yr between 1856 CE and 2014 CE, including 3.0 ± 0.3 mm/yr from 1900 CE to 2012 CE (Figures 2A and 7C; Kopp, 2013). This instrumental rate of RSL rise exceeds the long-term (~4000 years before present to 1900 CE) average estimated from compilations of RSL reconstructions from the Hudson River (1.2 ± 0.1 mm/yr) and Long Island (1.0 ± 0.3 mm/yr) regions that are adjacent to New York City (Engelhart and Horton, 2012; Engelhart et al., 2011). The similarity between these long-term rates of RSL rise and continuous measurements made by GPS stations (1.1 ± 0.2 mm/yr for Hudson River and 1.0 ± 0.2 mm/yr for Long Island) indicates that late Holocene RSL change was driven primarily by GIA-induced subsidence (Karegar et al., 2016) . This difference exists at locations with tide-gauge records and RSL reconstructions along the U.S. Atlantic coast (e.g., Engelhart et al., 2009; Kopp, 2013) and elsewhere (e.g., Shennan and Woodworth, 1992; Woodworth et al., 2009).

The relatively coarse resolution and fragmentary nature of Holocene sea-level index points (e.g., Engelhart and Horton, 2012) prohibits using them to precisely constrain the when modern rates of RSL rise were initiated. Near-continuous and high-resolution records of RSL change produced from salt-marsh sediment and spanning the last ~500 years or more provide a means to investigate when this change in rate began and how its expression varies among regions. Change point analysis of the Pelham Bay RSL reconstruction shows that the rate of rise increased at 1852-1911 CE (95% credible interval), which is consistent with other salt-marsh reconstructions from the U.S. Atlantic coast in Florida (1834-1922 CE), North Carolina (1865-1892 CE), New Jersey (1830-1873 CE), and Connecticut (1850-1886 CE; Figure 7B). Kemp et al. (2015)

identified the common interval for this change in rate as 1865-1873 CE and showed that the recent (last 100-150 years) rate of RSL rise at each of

these locations was markedly faster than any century-scale trend reconstructed in the late Holocene. The Pelham Bay RSL further supports this interpretation. Similarly, the global mean sea-level reconstruction of Kopp et al. (2016) demonstrated that historic rates of sea-level rise were initiated around 1860 CE and led to the 20th century experiencing a faster rise than any of the preceding 27 centuries. We conclude that the increased rates of RSL rise reconstructed and observed along the U.S. Atlantic coast are the regional expression of a global sea-level rise caused primarily by thermal expansion and the melting of mountain glaciers (Church et al., 2013) in response to warming that began in the mid-19th century (e.g., Mann et al., 2008).

Prior to the onset of modern rates of sea-level rise in the middle to late 19th century, the Pelham Bay RSL reconstruction includes periods when the rate of RSL rise was accelerating (approximately 800-1400 CE) and decelerating (approximately 1400-1800 CE; Figure 7C). A reconstruction from Connecticut identified a rate of rise in excess of background GIA at approximately 500-1100 CE, compared to 100-1000 CE in southern New Jersey and 900-1400 CE in North Carolina. Intervals of RSL rise less than background GIA occurred at approximately 1200-1700 CE in Connecticut, 1000-1600 in New Jersey, and 1400-1800 CE in North Carolina. In contrast, both of these features were absent in a reconstruction from northeastern Florida (summarized in figure 8 of Kemp et al., 2015). This spatial pattern of sea-level variability in the mid-Atlantic and northeastern United States compared to relative stability along the southeastern coast is characteristic of ocean dynamic effects predicted by models (Levermann et al., 2005; Yin et al., 2009) and is observed in instrumental data on annual to decadal timescales (Ezer,

2015; Goddard et al., 2015). Specifically, accelerating/decelerating sea-level rise at locations north of Cape Hatteras occurs when the dynamic sea-level gradient sustained by geostrophic flow of the Gulf Stream is relaxed/enhanced. The Pelham Bay reconstruction indicates that late Holocene rates of RSL rise varied on century timescales and conform to a broad spatial pattern which suggests that dynamic ocean circulation was a driver of regional sea-level trends during the past 1500 years. However, the asynchronous timing of late Holocene trends among sites north of Cape Hatteras complicates this interpretation and may be the product of local-scale processes at some sites.

5.2 Tidal-range change

The RSL reconstruction from Pelham Bay assumed that no-tidal range change occurred during the period under consideration (i.e. that the modern, observable tidal range has persisted for at least the past ~1500 years). Modeling of paleotides on the U.S. Atlantic coast indicates that this assumption is reasonable at the basin scale since ~7000 years ago (Hill et al., 2011; Griffiths and Hill, 2015). However, at smaller spatial scales (including Long Island Sound) this assumption has not been evaluated. To investigate the potential magnitude of tidal-range change at Pelham Bay, we ran a series of 35-day tidal simulations for Long Island Sound using the Stevens Institute Estuarine and Coastal Ocean model (sECOM) on the New York Harbor Observing and Prediction System (NYHOPS) domain (Georgas and Blumberg, 2009; Georgas et al., 2014; Orton et al., 2012). Theses simulations included only the astronomical constituents (M2, S2, N2, K2, K1, O1, Q1) and shallow-water, overtide constituents (M4, M6) that are provided to this model domain as open-boundary conditions at the edge of the continental shelf. In 16 model runs, we changed RSL in Long Island Sound by 0.25 m increments from -2.5 m (lower than

present) to +1.25 m (higher than present) and assumed that these changes were not accompanied by bathymetric or bottom-

friction changes from sediment infilling and/or anthropogenic activities (e.g., Brandon et al., 2016), i.e. the change in RSL is equal to the change in depth.

From each simulation we used the constituent amplitudes and phases (extracted by the Matlab program t_tide; Pawlowicz et al., 2002; Leffler and Jay, 2009) to construct a full 19-year nodal cycle tidal prediction dataset at Kings Point from which tidal datums such as MHHW were calculated. These simulations indicate that there is a strong (r^2>0.99), positive and near-linear relationship between the bathymetric depth of Long Island Sound and the great diurnal tidal range at Kings Point (Figure 8A). A linear regression between -2.5 m and 0 m relative depth estimates that great diurnal tidal range increases at ~0.09 m per meter change in depth. Instrumental measurements at Willets Point show that a ~0.35 m RSL rise since 1892 CE increased great diurnal tidal range by ~0.05 m, which is broadly comparable with our model results. Based on model simulations and historic tidal data we infer that RSL rise likely increased tidal range in Long Island Sound over the last 1500 years.

To estimate the possible impact of tidal-range change on the Pelham Bay RSL reconstruction, we generated a “base” RSL history (Figure 8B) by assuming that RSL rise since 1850 CE occurred at 2.84 mm/yr (the linear rate recorded by the Battery tide gauge) compared to 1.2 mm/yr for the period from ~500 CE to 1850 CE (e.g., Engelhart et al., 2009; Kopp et al., 2014; Karegar et al., 2016). For each year in this time series we estimated a paleo tidal range at Kings Point from our simulations. These time-varying tidal statistics were then applied to the PME reconstructions generated by the Bayesian transfer function (taking the mean, reconstructed sample age as true) to produce a RSL reconstruction that is adjusted for the effects of non-stationary tides (Figure

n an average difference between the RSL reconstructions of 0.05 m (up to 0.11 m; Figure 8C), but does not materially alter the reconstructed RSL trends.

Considering that the average (2σ) uncertainty in the original RSL reconstruction with stationary tides was ± 0.19 m, the two RSL reconstructions in Figure 8b are statistically indistinguishable from one another. Furthermore, the modeled changes in bathymetric depth (and hence changes to tidal statistics through time) are likely over-estimated because they do not consider sedimentation and our estimate of tidal-range change is therefore pessimistic. Late Holocene RSL rise in Long Island Sound was likely accompanied by sediment accretion at rates of up to ~1 mm/yr (e.g., Lewis and Mary, 2000; Varekamp et al., 2000; Kim and Bokuniewicz, 1991; Benoit et al., 1979; Bokuniewicz et al., 1976), which is sufficient to keep pace with long-term rates of RSL rise driven by GIA. On recent and shorter timescales, sediment supply to Long Island Sound probably spiked during regional deforestation (e.g., Kirwan et al., 2011) as evidenced by an increased rate of sediment accumulation at Pelham Bay from ~1600 CE onwards (Figure 5D). The rate of RSL since the late 19th century (Figure 7) likely exceeds sediment supply rates and resulted in depth changes, as indicated by the historical tidal-range measurements at Willets Point (Figure 8A). However, other anthropogenic changes such as loss of wetlands may also be contributing to measured tidal range changes. Therefore, the non-stationary tide RSL reconstruction (Figure 8B) is an outer bound estimate and the likely difference between the scenarios is smaller than depicted in Figure 8C. We conclude that the original reconstruction with stationary tides is representative of long-term, century-scale RSL trends.

52

To ascertain whether other nearby locations are affected by changes in tidal range, we repeated this analysis for four other sites

(Atlantic City and Sandy Hook, NJ; The Battery, NY; New Haven, CT; Figure 8D). These results show that changing bathymetric depth has little effect on great diurnal tidal range outside of Long Island Sound (with the caveat that we did not consider changes in wetland area). We therefore conclude that RSL reconstructions from the coast of New Jersey (e.g., Kemp et al., 2013a) are unlikely to be distorted by tidal-range change, but that its possible effect on records from Long Island Sound (e.g., Donnelly et al., 2004; Nydick et al., 1995; Kemp et al., 2015; van de Plassche et al., 1998) should be evaluated when reconstructing RSL.

5.3 Implications for 21st century sea-level change in New York City

The amount of RSL rise projected for New York City by 2100 CE exceeds the global mean because of local- to regional-scale contributions from ongoing GIA (e.g., Roy and Peltier, 2015), the fingerprint of West and East Antarctic ice-sheet melt (e.g., Mitrovica et al., 2009), ocean dynamics (e.g., Ezer et al., 2013; Yin and Goddard, 2013; Levermann et al., 2005), and spatially-variable thermal expansion arising from uneven uptake of heat by the oceans (e.g., Krasting et al., 2016). Under three climate scenarios, Miller et al. (2013) predicted RSL rise at The Battery by 2100 CE to be 0.64 m, 0.96 m, and 1.68 m above a 2000 CE baseline under their low, central, and high scenarios respectively. These projections are similar to those made by other groups for The Battery including the New York Panel on Climate Change (Horton et al., 2015; Kopp et al., 2014).

52

response to such short-lived trends and because the sediment slices used to produce the reconstruction are time averaged (for example, the average amount of time represented by a

To achieve even the optimistic, low-end scenario for 2100 CE the rate of RSL rise in New York City must accelerate during the 21st century. The validity of such RSL projections has been challenged in some quarters because the fitting of quadratic regressions to individual and compiled tide-gauge records often yields sea-level accelerations that cannot be distinguished from zero (e.g., Houston and Dean, 2011; Maul, 2015). However, this approach to analyzing tide-gauge records for evidence of an acceleration is hampered by the length of the available record (or selective use of start date) and the degree to which a quadratic form is appropriate for describing the sea-level trend under consideration (e.g., Rahmstorf and Vermeer, 2011). Haigh et al. (2014) showed that the acceleration of RSL rise at The Battery was ~0.008 mm/yr^2 over the period 1856-2009 CE, but was indistinguishable from zero (i.e. no detectable acceleration) if only data from 1880-2009 CE (for example) were analyzed. They concluded that individual tide-gauge records shorter than ~130 years were unlikely to show accelerations because of the noise introduced by annual to decadal variability. By simulating noisy tide-gauge data to 2100 CE under scenarios of global sea-level rise, they concluded that accelerations in the rate of RSL rise at specific locations would only become widely detectable in the 2020s or 2030s.

Proxy RSL reconstructions from salt marshes have two distinct advantages over tide gauge records for detecting accelerations in the rate of RSL rise. Firstly, they do not preserve the high-resolution (annual to decadal) "noise" that characterizes individual tide-gauge records (and to a lesser extent global compilations; e.g., Church and White, 2011; Hay et al., 2015) because biological sea-level proxies such as foraminifera and plants do not achieve an equilibrium response to such short-lived trends and because the sediment slices used to produce the reconstruction are time averaged (for example, the average amount of time represented by a

52

risk from RSL rise in communities bordering Long Island Sound because the elevation of high tides will increase more than RSL. For example, at Willet's Point, the modeled increase in e only multi-decadal trends (e.g., Kemp et al., 2011; Barlow et al., 2013). Secondly, they are unhindered by the available record length, meaning that it could be possible to detect accelerating sea-level rise now rather than waiting for additional years of measurements, which may delay efforts to plan for, or manage the effects of, future sea-level rise. Unlike the fitting of quadratic or polynomial functions, the EIV-IGP and change-point models that we used to quantify sea-level trends at Pelham Bay account for temporal and vertical uncertainties and the uneven distribution of data points through time to provide continuous estimates of rate with uncertainty (Cahill et al., 2015a). Analysis of the Pelham Bay reconstruction shows that the rate of RSL rise increased (i.e. sea-level rise accelerated) continually since ~1700 CE due to natural warming at the end of the Little Ice Age and then from additional forcing by recent climate change. A similar analysis of global tide-gauge records (Church and White, 2011; Jevrejeva et al., 2008) also showed acceleration throughout the 20th century (Cahill et al., 2015a: ; Figure 8A). Contrary to simple analysis of tide-gauge records, we conclude that the significant acceleration necessary for RSL in New York City to reach the heights projected for 2100 CE and beyond is already underway.

In contrast to the late Holocene, future RSL rise in New York City is likely to exceed the rate of sediment accumulation in Long Island Sound and cause an increase in bathymetric depth. Observational data from Willets Point and our tidal simulations suggest that future deepening of Long Island Sound will increase tidal range (Figure 8). This change will exacerbate the flood risk from RSL rise in communities bordering Long Island Sound because the elevation of high tides will increase more than RSL. For example, at Willet's Point, the modeled increase in

1-cm thick slice of PBA-4 is approximately one decade). Reconstructions of RSL from salt marsh sediment are consequently naturally-filtered records that preserv

se of ~1 m (the central projection of Miller et al., 2013), while the increase at New Haven is ~8%. In contrast, the increase at the Battery in New York Harbor is ~3%. Therefore local-scale planning for 21st-century RSL rise within New York City should include explicit consideration of tidal-range change which will result in spatially-variable flood risk.

6. CONCLUSIONS

Low-lying areas of New York City are at risk from regional relative sea-level rise that will exceed the global mean. To understand the late Holocene sea-level history of New York City we produced a relative sea-level reconstruction using a sediment core collected from an urban salt marsh in Pelham Bay (The Bronx). Within a Bayesian hierarchical model foraminifera and bulk-sediment $\delta^{13}C$ values were employed as sea-level indicators and an age-depth model was generated from a composite of chronology comprised of radiocarbon ages and marker horizons identified from elemental, isotopic and pollen profiles that reflect pollution and land-use trends of known age. The resulting reconstruction shows that RSL rose by ~1.70 m since ~575 CE. Modeling of the relationship between the depth of Long Island Sound and tidal range at Pelham Bay indicates that paleo tidal-range change is unlikely to have materially affected the new reconstruction. A pronounced acceleration in the rate of relative sea-level rise began at 1852-1911 CE and is consistent with other reconstructions and measurements made in the western North Atlantic Ocean. The current rate of rise is the fastest to have occurred for at least 1500 years and the strong acceleration of RSL rise that is necessary to realize projections for 2100 CE is likely underway. Future tidal-range change caused by deepening of Long Island

most vulnerable to flooding by high tides.

Sound will likely cause local-scale differences in flood risk within New York City with communities bordering Long Island Sound being the

7. ACKNOWLEDGEMENTS

We thank Christopher Bernhardt (USGS) for his assistance with the pollen analysis. Kemp thanks a post-doctoral fellowship from the Yale University Climate and Energy Institute, the mentoring of Shimon Anisfeld, NOAA award NA11OAR4310101 and NSF award OCE-MGG- 1458921. Talke was funded by the U.S. Army Corps of Engineers (Award W1927N-14-2-0015) and NSF awards 1455350 and OCE-1155610. Orton was funded under NOAA's Regional Integrated Sciences and Assessments (RISA) program (award NA10OAR4310212). This work is a contribution to PALSEA 2 and IGCP Project 639, "*Sea-level change from minutes to millennia*". Access to the Pelham Bay study site was facilitated by the New York City Department of Parks & Recreation.

4. $\delta^{13}C$ was measured on a CO_2 aliquot from the combusted sample and is expressed relative to the Vienna Pee Dee Belemnite (VPDB) standard. All samples underwent standard acid-base-acid pretreatment prior to radiocarbon measurement by accelerator mass spectrometry.

Table One: Radiocarbon dates from Pelham Bay core 4 (PBA-4).

Depth in Core (cm)	Sample ID	Age (^{14}C years)	Age Error (^{14}C years)	$\delta^{13}C$ (‰, VPDB)	Sample Description
60	OS-102551	165	25	-13.91	*Distichlis spicata* rhizome
70	OS-108259	380	30	-23.56	Unidentified rhizome
81	OS-108260	285	25	-25.21	*Phragmites australis* stem
95	OS-102552	770	30	-12.92	*Distichlis spicata* rhizome
105	OS-115123	695	20	-24.82	*Phragmites australis* stem
123	OS-109016	1420	30	-14.19	*Distichlis spicata* rhizome
127	OS-115122	1120	15	-13.45	*Distichlis spicata* rhizome
137	OS-102598	1180	35	-25.50	Acorn cupule
155	OS-102553	1560	25	-28.43	*Phragmites australis* stem
161	OS-102554	1630	35	-27.92	Small piece of wood

Radiocarbon ages reported by the National Ocean Sciences Mass Spectrometry laboratory for macrofossil samples isolated from PBA-

the Pelham Bay study site in The Bronx, New York City (NYC) and National Oceanic and Atmospheric Administration (NOAA) tide gauges (numbered blue circles in panel A). The inset in panel A shows the location of NYC and other proxy relative sea-level reconstructions (Connecticut, New Jersey, North Carolina and Florida) on the U.S. Atlantic coast. **(D)** Sediment beneath the Pelham Bay salt marsh described from cores recovered along two transects (A-A' and B-B'). Core number 4 (PBA-4) was selected for detailed analysis because it included the thickest sequence of peat and was representative of the stratigraphy at the site.

FIGURE CAPTIONS

Figure 1: (A-C) Location of

Figure 2: (A) Relative sea level measured by tide gauges in New York City. Annual data from The Battery, Willets Point and New Rochelle up to and including 2014 were downloaded from the Permanent Service for Mean Sea Level. The Battery is located at the southern tip of Manhattan and measures RSL in New York Harbor. The instruments at Willets Point and New Rochelle record RSL in Long Island Sound. Average RSL over the period 1960-1969 CE is the reference period for each tide gauge series. Monthly data (January 1999 to December 2014) for Kings Point were downloaded from the National Ocean and Atmospheric Administration and used to generate annual averages that in turn were referenced the RSL at The Battery. **(B)** Correlation between tides measured at the Pelham Bay field site using an automated water logger (relative to the North American Vertical Datum of 1988; NAVD88) and those measured by the NOAA-operated tide gauge at Kings Point with respect to local mean higher high water (MHHW). At Willets Point MHHW lies 1.13 m above NAVD88.

Figure 3: Assessment of the Bayesian transfer function's (B-TF) performance using cross validation. The modern training set was comprised of 254 samples from 12 salt marshes (including Pelham Bay) on the Long Island Sound coast of New York and Connecticut. **(A)** Comparison of actual elevations measured at the time of sample collection and predicted by the B-TF with 95% credible intervals. Dashed line represents parity between actual and predicted elevations. **(B)** Difference between actual and mean predicted elevations. MTL = mean tide level, MHHW = mean higher high water, HOF = highest occurrence of foraminifera in the modern training set, SWLI = standardized water level index.

Figure 4: Sea-level indicators and paleomarsh elevation (PME) reconstructions from PBA-4. **(A)** Total organic carbon measured on bulk-sediment samples. **(B)** Relative abundance of the four most common species of foraminifera. For consistency with the modern training set, counts of *Trochammina inflata* and *Siphotrochammina lobata* were combined prior to analysis. Samples represented by grey bars had counts of fewer than 50 foraminifera and were excluded from the final relative sea level reconstruction. **(C)** Measurements of $\delta^{13}C$ in bulk-sediment samples relative to the Vienna Pee Dee Belemnite (VPDB) standard. Shaded areas denote values associated with environments dominated by C_4 and C_3 plant species. Symbol shading denotes the prior constraint placed on PME in the Bayesian transfer function based on the modern distribution of C_4 and C_3 plant communities on and around salt marshes in New Jersey, USA.
(D) Paleomarsh elevation (mean with 95% credible interval) estimated using the Bayesian transfer function including the prior constraint provided by bulk sediment $\delta^{13}C$ measurements. Symbol shading denotes the prior placed on each sample based on bulk-sediment $\delta^{13}C$ measurements. SWLI = standardized water level index, HOF = highest occurrence of

foraminifera, MHHW = mean higher high water. **(E)** Dissimilarity between core samples and their closest modern analogue in the modern training set measured using the Bray Curtis metric. Dashed vertical lines represent percentiles of dissimilarity measured for all possible pairs of modern samples. Core samples exceeding the 20% threshold were excluded from the reconstruction (grey shaded area). The 10% threshold is shown for comparison. Symbol colors denote the site that provided the closest modern analogue. CIC = Canfield Island Cove, PBB = Pelham Bay, HRM = Hammock River Marsh, PAT = Pattagansett, MKA = Menunketesuk, ERM = East River Marsh, EBD = East Branford, MC = Marsh Conservancy, GPE= Gulf Pond East, DB = Double Beach.

Figure 5: Chronology for PBA-4. Measurement uncertainties are smaller than symbols. Shaded envelopes represent the depth (with uncertainty) of each chronohorizon. Assigned ages with uncertainty are listed. **(A)** Elemental and isotopic profiles used to identify regional-scale pollution markers. **(B)** Suite of elemental profiles used to identify a local-scale pollution marker caused by incineration of domestic waste at sites throughout New York City in the early 20th century. **(C)** Recognition of a land-use marker horizon associated with clearance by European settlers from pollen profiles and the down core concentration of titanium and potassium. **(D)** Bchron age-depth model developed for PBA-4 (mean and 95% credible interval). Calibrated (2σ) radiocarbon ages are represented by grey bars thicknesses that are proportional to their probability. Inset shows last ~200 years in more detail.

Figure 6: (A) Annual sedimentation rates for core PBA-4 estimated from the suite of chronologies generated by the Bchron age-depth model. Results are the mean (solid line) and

90% credible interval (5^{th} to 95^{th} percentiles; shaded envelope). (B) Comparison of late Holocene annual sediment

ation rates from salt marshes in Connecticut, New York City and southern New Jersey. Sedimentation rates were estimated by applying the same approach to each dataset. For clarity of presentation only mean estimates are presented and details of sedimentation rates during the past ~250 years are shown in detail in the inset panel.

Figure 7: Relative sea level (RSL) reconstruction from Pelham Bay in New York City. **(A)** Proxy reconstructions are represented by boxes that encompass vertical and chronological uncertainties. Only 1σ uncertainties are shown for clarity, but subsequent analysis used the 2σ uncertainties. Annual RSL measurements from The Battery tide gauge were reduced to decadal averages (red line) and combined with the salt-marsh reconstruction from PBA-4 to provide a proxy and instrumental record of RSL change in New York City. **(B)** Results from the Errors-in-Variables Integrated Gaussian Process (EIV-IGP) model displayed as a mean with shading denoting the 68% and 95% credible intervals. For clarity of presentation reconstructions are represented by their mid points only. Vertical shaded regions show the timing of significant change points at 1015-1238 CE and 1852-1911 CE (95% credible ranges). Red bars show timing of historic change points identified in proxy RSL reconstructions from Connecticut (CT), New Jersey (NJ), North Carolina (NC) and Florida (FL) and reported by Kemp et al. (2015). **(C)** Rate of RSL change estimated by the EIV-IGP model presented as a mean with shaded 68% and 95% credible intervals. Positive values refer to RSL rise. The green shaded envelope marks the average rate of RSL rise measured by The Battery tide gauge from 1900-2012 and reported by Kopp (2013), while the dashed red line marks the average linear rate of rise reported by the National Ocean and Atmospheric Administration (NOAA). Dashed grey lines (mean) and

shaded grey area (uncertainty

) represent the regional background rates of late Holocene RSL rise estimated by Engelhart and Horton (2012) for the Hudson River (1.25 ± 0.1 mm/yr) and Long Island (1.0 ± 0.3 mm/yr) regions and attributed primarily to ongoing glacio-isostatic adjustment.

Figure 8: **(A)** Great diurnal tidal range (mean lower low water to mean higher high water) simulated for Kings Point using the Coastal Ocean model (open circles) with sea level varying from -2.5 m (shallower depths than present) to + 1.25 m (deeper than present). Historic measurements from the Willets Point tide gauge (filled diamonds) are shown for comparison, where measured relative sea level (RSL) change is assumed to correspond to a change in depth. **(B)** Effect of tidal-range change on the Pelham Bay RSL. The original RSL reconstruction assumes a constant tidal range during the past 1500 years (open circles). This reconstruction was adjusted for non-stationary tides (filled circles) by using an assumed RSL history (dashed line) in which the pre-1850 trend is driven solely by glacio-isostatic adjustment at 1.2 mm/yr and the post-1850 trend is provided by RSL measurements at the Battery in New York City. A paleo tidal range was estimated for each year in the "base" RSL history using the tidal simulations for Kings Point under the assumption that RSL change caused a corresponding depth change in Long Island Sound. **(C)** Difference in RSL between the original reconstruction and the one conservatively adjusted for possible tidal-range change. **(D)** Percentage change in great diurnal tidal range (negative values indicate a smaller tidal range than present) simulated to occur at five tide-gauge locations when water depth is varied by -2.5 to + 1.25 m. The current range at each location is provided in the legend.

REFERENCES

Anisfeld SC, Tobin MJ and Benoit G. (1999) Sedimentation rates in flow-restricted and restored salt marshes in Long Island Sound. *Estuaries* 22: 231-244.

Barlow NLM, Shennan I, Long AJ, et al. (2013) Salt marshes as late Holocene tide gauges. *Global and Planetary Change* 106: 90-110.

Benoit GJ, Turekian KK and Benninger LK. (1979) Radiocarbon dating of a core from Long Island sound. *Estuarine and Coastal Marine Science* 9: 171-180.

Bokuniewicz HJ, Gebert J and Gordon RB. (1976) Sediment mass balance of a large estuary, Long Island Sound. *Estuarine and Coastal Marine Science* 4: 523-536.

Bollhöfer A and Rosman KJR. (2001) Isotopic source signatures for atmospheric lead: the Northern Hemisphere. *Geochimica et Cosmochimica Acta* 65: 1727-1740.

Brandon CM, Woodruff JD, Orton PM, et al. (2016) Evidence for elevated coastal vulnerability following large-scale historical oyster bed harvesting. *Earth Surface Processes and Landforms*: n/a-n/a.

Bricker-Urso S, Nixon SW, Cochran JK, et al. (1989) Accretion rates and sediment accumulation in Rhode Island salt marshes. *Estuaries* 12: 300-317.

Brugam RB. (1978) Pollen indicators of land-use change in southern Connecticut. *Quaternary Research* 9: 349-362.

Burrows EG and Wallace M. (1999) *Gotham: a history of New York City to 1898,* New York, New York: Oxford University Press.

Cahill N, Kemp AC, Horton BP, et al. (2015a) Modeling sea-level change using errors-in-variables intergrated Gaussian processes. *Annals of Applied Statistics* 9: 547-571.

Cahill N, Kemp AC, Parnell AC, et al. (2016) A Bayesian hierarchical model for reconstructing relative sea level: from raw data to rates. *Climate of the Past* 12: 525-542.

Cahill N, Rahmstorf S and Parnell AC. (2015b) Change points of global temperature. *Environmental Research Letters* 10: 084002.

Carlin BP, Gelfand AE and Smith AFM. (1992) Hierarchical Bayesian analysis of changepoint problems. *Applied Statistics* 41: 389-405.

Chillrud SN, Bopp RF, Simpson HJ, et al. (1999) Twentieth century atmospheric metal fluxes into Central Park Lake, New York City. *Environmental Science & Technology* 33: 657-662.

Chmura GL and Aharon P. (1995) Stable carbon isotope signatures of sedimentary carbon in coastal wetlands as indicators of salinity regime. *Journal of Coastal Research* 11: 124-135.

Church JA, Clark PU, Cazenave A, et al. (2013) Sea-level change. In: Stocker TF, D. Qin D, Plattner GK, et al. (eds) *Climate Change 2013: The Physical Science Basis. Contribution of Working Group I to the Fifth Assessment Report of the Intergovernmental Panel on Climate Change.* Cambridge University Press, 1137-1216.

Church JA and White NJ. (2011) Sea-level rise from the late 19th to the early 21st century. *Surveys in Geophysics* 32: 585-602.

Cochran JK, Hirschberg DJ, Wang J, et al. (1998) Atmospheric deposition of metals to coastal waters (Long Island Sound, New York U.S.A.): evidence from saltmarsh deposits. *Estuarine, Coastal and Shelf Science* 46: 503-522.

Davis JL and Mitrovica JX. (1996) Glacial isostatic adjustment and the anomalous tide gauge record of

9-425.

Donnelly JP. (2006) A revised late Holocene sea-level record for northern Massachusetts, USA. *Journal of Coastal Research* 22: 1051-1061.

eastern North America. *Nature* 379: 331-333.

Doe BR and Delevaux MH. (1972) Source of Lead in southeast Missouri Galena ores. *Economic Geology* 67: 40

Donnelly JP and Bertness MD. (2001) Rapid shoreward encroachment of salt marsh cordgrass in response to accelerated sea-level rise. *Proceedings of the National Academy of Sciences of the United States of America* 98: 14218-14223.

Donnelly JP, Cleary P, Newby P, et al. (2004) Coupling instrumental and geological records of sea-level change: evidence from southern New England of an increase in the rate of sea-level rise in the late 19th century. *Geophysical Research Letters* 31: L05203.

Edwards RJ and Wright AJ. (2015) Foraminifera. In: Shennan I, Long AJ and Horton BP (eds) *Handbook of Sea-Level Research.* John Wiley & Sons, 191-217.

Edwards RJ, Wright AJ and van de Plassche O. (2004) Surface distributions of salt-marsh foraminifera from Connecticut, USA: modern analogues for high-resolution sea level studies. *Marine Micropaleontology* 51: 1-21.

Engelhart SE and Horton BP. (2012) Holocene sea level database for the Atlantic coast of the United States. *Quaternary Science Reviews* 54: 12-25.

Engelhart SE, Horton BP, Douglas BC, et al. (2009) Spatial variability of late Holocene and 20th century sea-level rise along the Atlantic coast of the United States. *Geology* 37: 1115-1118.

Engelhart SE, Horton BP and Kemp AC. (2011) Holocene sea level changes along the United States' Atlantic Coast. *Oceanography* 24: 70-79.

Ezer T. (2015) Detecting changes in the transport of the Gulf Stream and the Atlantic overturning circulation from coastal sea level data: The extreme decline in 2009–2010 and estimated variations for 1935–2012. *Global and Planetary Change* 129: 23-36.

Ezer T, Atkinson LP, Corlett WB, et al. (2013) Gulf Stream's induced sea level rise and variability along the U.S. mid-Atlantic coast. *Journal of Geophysical Research: Oceans* 118: 685-697.

Facchetti S. (1989) Lead in petrol. The isotopic lead experiment. *Accounts of Chemical Research* 22: 370-374.

Fuller LJ, Foster RD, McLachlan SJ, et al. (1998) Impact of human activity on regional forest composition and dynamics in central New England. *Ecosystems* 1: 76-95.

Gehrels WR. (1994) Determining relative sea-level change from salt-marsh foraminifera and plant zones on the coast of Maine, U.S.A. *Journal of Coastal Research* 10: 990-1009.

Gehrels WR. (2000) Using foraminiferal transfer functions to produce high-resolution sea-level records from salt-marsh deposits, Maine, USA. *The Holocene* 10: 367-376.

Gehrels WR, Kirby JR, Prokoph A, et al. (2005) Onset of recent rapid sea-level rise in the western Atlantic Ocean. *Quaternary Science Reviews* 24: 2083-2100.

Gehrels WR and van de Plassche O. (1999) The use of *Jadammina macrescens* (Brady) and *Balticammina pseudomacrescens* Brönnimann, Lutze and Whittaker (Protozoa: Foraminiferida) as sea-level indicators. *Palaeogeography, Palaeoclimatology, Palaeoecology* 149: 89-101.

Gehrels WR and Woodworth PL. (2012) When did modern rates of sea-level rise start? *Global and Planetary Change* 100: 263-277.

Georgas N and Blumberg AF. (2009) Establishing Confidence in M
Skill Assessment of the New York Harbor Observation anc
v3). *Eleventh International Conference in Estuarine and C*

Georgas N, Orton P, Blumberg A, et al. (2014) The impact of tidal phase on Hurricane Sandy's flooding around New York City and Long Island Sound. *Journal of Extreme Events* 1: 1450006.

Gobeil C, Tessier A and Couture R-M. (2013) Upper Mississippi Pb as a mid-1800s chronostratigraphic marker in sediments from seasonally anoxic lakes in Eastern Canada. *Geochimica et Cosmochimica Acta* 113: 125-135.

Goddard PB, Yin J, Griffies SM, et al. (2015) An extreme event of sea-level rise along the Northeast coast of North America in 2009–2010. *Nature Communications* 6.

Gomez N, Mitrovica JX, Tamisiea ME, et al. (2010) A new projection of sea level change in response to collapse of marine sectors of the Antarctic Ice Sheet. *Geophysical Journal International* 180: 623-634.

Gornitz V, Couch S and Hartig EK. (2001) Impacts of sea level rise in the New York City metropolitan area. *Global and Planetary Change* 32: 61-88.

Graney JR, Halliday AN, Keeler GJ, et al. (1995) Isotopic record of lead pollution in lake sediments from the northeastern United States. *Geochimica et Cosmochimica Acta* 59: 1715-1728.

Griffiths SD and Hill DF. (2015) Tidal Modeling. In: Shennan I, Long AJ and Horton BP (eds) *Handbook of Sea-Level Research.* John Wiley and Sons, 438-451.

Haigh ID, Wahl T, Rohling EJ, et al. (2014) Timescales for detecting a significant acceleration in sea level rise. *Nature Communications* 5: 1-11.

Haroun M, Idris A and Syed Omar SR. (2007) A study of heavy metals and their fate in the composting of tannery sludge. *Waste Management* 27: 1541-1550.

Harrison EZ and Bloom AL. (1977) Sedimentation rates on tidal salt marshes in Connecticut. *Journal of Sedimentary Research* 47.

Hartig E, Gornitz V, Kolker A, et al. (2002) Anthropogenic and climate-change impacts on salt marshes of Jamaica Bay, New York City. *Wetlands* 22: 71-89.

Haslett J and Parnell A. (2008) A simple monotone process with application to radiocarbon-dated depth chronologies. *Journal of the Royal Statistical Society: Series C (Applied Statistics)* 57: 399-418.

Hay C, Morrow E, Kopp RE, et al. (2015) Probabilistic reanalysis of twentieth-century sea-level rise. *Nature* 517: 481-484.

Heyl AV, Delevaux MH, Zartman RE, et al. (1966) Isotopic study of galenas from the upper Mississippi Valley, the Illinois-Kentucky, and some Appalachian Valley mineral districts. *Economic Geology* 61: 933-961.

Heyl AV, Landis GP and Zartman RE. (1974) Isotopic Evidence for Mineral Deposits: A Review. *Economic Geology* 69: 992-

Hill DF, Griffiths SD, Peltier WR, et al. (2011) High-resolution nun

Research 116.

Hill TD and Anisfeld SC. (2015) Coastal wetland response to sea level rise in Connecticut and New York. *Estuarine, Coastal and Shelf Science* 163, Part B: 185-193.

Horton BP and Edwards RJ. (2005) The application of local and regional transfer functions to the reconstruction of Holocene sea levels, north Norfolk, England. *Holocene* 15: 216-228.

Horton BP and Edwards RJ. (2006) Quantifying Holocene sea-level change using intertidal foraminifera: lessons from the British Isles. *Cushman Foundation for Foraminiferal Research, Special Publication* 40: 97.

Horton R, Little C, Gornitz V, et al. (2015) New York City Panel on Climate Change 2015 Report Chapter 2: Sea Level Rise and Coastal Storms. *Annals of the New York Academy of Sciences* 1336: 36-44.

Houston JR and Dean RG. (2011) Sea-level acceleration based on U.S. tide gauges and extensions of

previous global-gauge analyses. *Journal of Coastal Research*: 409-417.
Hurst RW. (2000) Applications of anthropogenic lead archaeostratigraphy (ALAS model) to hydrocarbon remediation. *Environmental Forensics* 1: 11-23.
Jevrejeva S, Moore JC, Grinsted A, et al. (2008) Recent global sea level acceleration started over 200 years ago? *Geophysical Research Letters* 35: L08715.
Johnson BJ, Moore KA, Lehmann C, et al. (2007) Middle to late Holocene fluctuations of C_3 and C_4 vegetation in a Northern New England Salt Marsh, Sprague Marsh, Phippsburg Maine. *Organic Geochemistry* 38: 394-403.

Johnson DS and York HH. (1915) *The relation of plants to tide-levels; a study of factors affecting the distribution of marine plants,* Washington, D.C.: Carnegie Institution of Washington.
Juggins S and Birks HJB. (2012) Quantiative environmental reconstructions from biological data. In: Birks HJB, Lotter AF, Juggins S, et al. (eds) *Tracking environmental change using lake sediments: Data handling and numerical techniques.* Springer, 431-494.
Kamenov GD, Brenner M and Tucker JL. (2009) Anthropogenic versus natural control on trace element and Sr-Nd-Pb isotope stratigraphy in peat sediments of southeast Florida (USA), ~1500 AD to present. *Geochimica et Cosmochimica Acta* 73: 3549-3567.
Karegar MA, Dixon TH and Engelhart SE. (2016) Subsidence along the Atlantic Coast of North America: Insights from GPS and late Holocene relative sea level data. *Geophysical Research Letters* 43: 3126-3133.
Kelly AE, Reuer MK, Goodkin NF, et al. (2009) Lead concentrations and isotopes in corals and water near Bermuda, 1780-2000. *Earth and Planetary Science Letters* 283: 93-100.
Kemp AC, Bernhardt CE, Horton BP, et al. (2014) Late Holocene sea- and land-level change on the U.S. southeastern Atlantic coast. *Marine Geology* 357: 90-100.
Kemp AC, Hawkes AD, Donnelly JP, et al. (2015) Relative sea-level change in Connecticut (USA) during the last 2200 years. *Earth and Planetary Science Letters* 428: 217-229.
Kemp AC, Horton B, Donnelly JP, et al. (2011) Climate related sea-level variations over the past two millennia. *Proceedings of the National Academy of Sciences* 108: 11017-11022.
Kemp AC, Horton BP, Vane CH, et al. (2013a) Sea-level change during the last 2500 years in New Jersey, USA. *Quaternary Science Reviews* 81: 90-104.
Kemp AC, Sommerfield CK, Vane CH, et al. (2012a) Use of lead isotopes for developing chronologies in recent salt-marsh sediments. *Quaternary Geochronology* 12: 40-49.
Kemp AC and Telford RJ. (2015) Transfer Functions. In: Shennan I, Long AJ and Horton BP (eds) *Handbook for Sea-Level Research.* Wiley, 470-499.
Kemp AC, Telford RJ, Horton BP, et al. (2013b) Reconstructing Holocene sea-level using salt-marsh foraminifera and transfer functions: lessons from New Jersey, USA. *Journal of Quaternary Science* 28: 617-629.
Kemp AC, Vane CH, Horton BP, et al. (2012b) Application of stable carbon isotopes for reconstructing salt-marsh floral zones and relative sea level, New Jersey, USA. *Journal of Quaternary Science* 27: 404-414.
Kim B-H and Bokuniewicz HJ. (1991) Estimates of sediment fluxes in Long Island Sound. *Estuaries* 14: 237-247.
Kirwan ML and Murray AB. (2007) A coupled geomorphic and ecological model of tidal marsh evolution. *Proceedings of the National Academy of Sciences of the United States of America* 104: 6118-6122.
Kirwan ML and Murray AB. (2008) Tidal marshes as the disequilibrium landscapes: lags between morphology and Holocene sea level change. *Geophysical Research Letters* 35: L24401.
Kirwan ML, Murray AB, Donnelly JP, et al. (2011) Rapid wetland expansion during European settlement and its implication for marsh survival under modern sediment delivery rates. *Geology* 39: 507-510.
Kopp RE. (2013) Does the mid-Atlantic United States sea level acceleration hot spot reflect ocean dynamic variability? *Geophysical Research Letters* 40: 3981-3985.
Kopp RE, Horton RM, Little CM, et al. (2014) Probabilistic 21st and 22nd century sea-level projections at a global network of tide-gauge sites. *Earth's Future* 2: 383-406.
Kopp RE, Kemp AC, Bitterman K, et al. (2016) Temperature-driven global sea-level variability in the Common Era. *Proceedings of the National Academy of Sciences* 113: E1434-E1441.

ea-level rise relative to the Pacific under high carbon emission rates. *Nature Geoscience* 9: 210-214.
Lamb AL, Wilson GP and Leng MJ. (2006) A review of coastal palaeoclimate and relative sea-level reconstructions using $\delta^{13}C$ and C/N ratios in organic material. *Earth-Science Reviews* 75: 29-57.
Lang S and Brezger A. (2004) Bayesian P-splines. *Journal of computational and graphical statistics* 13: 183-212.
Leffler KE and Jay DA. (2009) Enhancing tidal harmonic analysis: robust (hybrid L1/L2) solutions. *Continental Shelf Research* 29: 78-88.
Levermann A, Griesel A, Hofmann M, et al. (2005) Dynamic sea level changes following changes in the thermohaline circulation. *Climate Dynamics* 24: 347-354.
Lewis RS and Mary D-C. (2000) A review of the geologic framework of the Long Island Sound basin, with some observations relating to postglacial sedimentation. *Journal of Coastal Research* 16: 522-532.
Lima AL, Bergquist BA, Boyle EA, et al. (2005) High-resolution historical records from Pettaquamscutt River basin sediments: 2. Pb isotopes reveal a potential new stratigraphic marker. *Geochimica et Cosmochimica Acta* 69: 1813-1824.
Mann ME, Zhang Z, Hughes MK, et al. (2008) Proxy-based reconstructions of hemispheric and global surface temperature variations over the past two millennia. *Proceedings of the National Academy of Sciences* 105: 13252-13257.
Marshall W. (2015) Chronohorizons: indirect and unique event dating methods for sea-level reconstructions. In: Shennan I, Long AJ and Horton BP (eds) *Handbook of Sea-Level Research.* Wiley, 373-385.
Maul GA. (2015) Florida's rising seas: a report in feet per century for coastal interests. *Florida Scientist* 78: 64-87.
McAndrews JH. (1988) Human disturbance of North American forests and grasslands: The fossil pollen record. In: Huntley B and Webb T (eds) *Vegetation history.* Dordrecht: Springer Netherlands, 673-697.
McCaffery RJ and Thomson J. (1980) A record of accumulation of sediment and trace metals in a Connecticut salt marsh. In: Saltzman B (ed) *Estuarine physics and chemistry: studies in Long Island Sond.* 22 ed. New York: Academic Press, 165-237.
Middleburg JJ, Nieuwenhuize J, Lubberts RK, et al. (1997) Organic carbon isotope systematics of coastal marshes. *Estuarine Coastal and Shelf Science* 45: 681-687.
Miller KG, Kopp RE, Horton BP, et al. (2013) A geological perspective on sea-level rise and its impacts along the U.S. mid-Atlantic coast. *Earth's Future*.
Mitrovica JX, Gomez N and Clark PU. (2009) The Sea-Level Fingerprint of West Antarctic Collapse. *Science* 323: 753.
Morris JT, Barber DC, Callaway JC, et al. (2016) Contributions of organic and inorganic matter to sediment volume and accretion in tidal wetlands at steady state. *Earth's Future* 4: 110-121.
Morris JT, Sundareshwar PV, Nietch CT, et al. (2002) Response of coastal wetlands to rising sea level. *Ecology* 83: 2869-2877.
Niering WA, Warren RS and Weymouth CG. (1977) Our dynamic tidal marshes: vegetation changes as revealed by peat analysis. *The Connecticut Arboretum Bulletin.* 22 ed., 12.
Nurse LA, McLean RF, Agard J, et al. (2014) Small islands. In: Barros VR, Field CB, Dokken DJ, et al. (eds) *Climate Change 2014: Impacts, Adaptation, and Vulnerability. Part B: Regional Aspects. Contribution of Working Group II to the Fifth Assessment Report of the Intergovernmental Panel of Climate Change.* Cambridge, United Kingdom and New York, NY, USA: Cambridge University Press, 1613-1654.

Nydick KR, Bidwell AB, Thomas E, et al. (1995) A sea-level rise curve from Guilford, Connecticut, USA. *Marine Geology* 124: 137-159.

Orton P, Georgas N, Blumberg A, et al. (2012) Detailed modeling of recent severe storm tides in estuaries of the New York City region. *Journal of Geophysical Research* 117: C09030.

Parnell AC, Haslett J, Allen JRM, et al. (2008) A flexible approach t using Bayesian reconstructions of sedimentation history. 1885 in MATLAB using T_TIDE. *Computers & Geosciences* 28: 929-937.

Pederson DC, Peteet DM, Kurdyla D, et al. (2005) Medieval Warming, Little Ice Age, and European impact on the environment during the last millennium in the lower Hudson Valley, New York, USA. *Quaternary Research* 63: 238-249.

Peltier WR. (2004) Global glacial isostasy and the surface of the ice-age Earth: the ICE-5G (VM2) model and GRACE. *Annual Review of Earth and Planetary Sciences* 32: 111-149.

Peterson BJ, Howarth RW and Garritt RH. (1985) Multiple stable isotopes used to trace the flow of organic matter in estuarine food webs. *Science* 227: 1361-1363.

Rahmstorf S and Vermeer M. (2011) Discussion of: Houston, J.R. and Dean, R.G., 2011. Sea-level acceleration based on U.S. tide gauges and extensions of previous global-gauge analyses. Journal of Coastal Research, 27(3), 409–417. *Journal of Coastal Research* 27: 484-487.

Reavie E and Juggins S. (2011) Exploration of sample size and diatom-based indicator performance in three North American phosphorus training sets. *Aquatic Ecology* 45: 529-538.

Redfield AC. (1972) Development of a New England salt marsh. *Ecological Monographs* 42: 201-237.

Reimer PJ, Bard E, Bayliss A, et al. (2013) IntCal13 and Marine13 Radiocarbon Age Calibration Curves 0–50,000 Years cal BP. *Radiocarbon* 55: 1869-1887.

Roman CT, Peck JA, Allen J, et al. (1997) Accretion of a New England (USA) salt marsh in response to inlet migration, storms, and sea-level rise. *Estuarine, Coastal and Shelf Science* 45: 717-727.

Roy K and Peltier WR. (2015) Glacial isostatic adjustment, relative sea level history and mantle viscosity: Reconciling relative sea level model predictions for the U.S. East coast with geological constraints. *Geophysical Journal International* 201: 1156-1181.

Saltonstall K. (2002) Cryptic invasion by a non-native genotype of the common reed, Phragmites australis, into North America. *Proceedings of the National Academy of Sciences* 99: 2445-2449.

Scott DB and Medioli FS. (1978) Vertical zonations of marsh foraminifera as accurate indicators of former sea levels. *Nature* 272: 528-531.

Scott DB and Medioli FS. (1980) Quantitative Studies of Marsh Foraminiferal Distributions in Nova Scotia: Implications for Sea Level Studies. *Cushman Foundation for Foraminiferal Research* 17.

Scott DB, Williamson MA and Duffett TE. (1981) Marsh foraminifera of Prince Edward Island: their recent distribution and application for former sea-level studies. *Maritime Sediments and Atlantic Geology* 17: 98-129.

Shennan I. (1986) Flandrian sea-level changes in the Fenland. II: Tendencies of sea-level movement, altitudinal changes, and local and regional factors. *Journal of Quaternary Science* 1: 155-179.

Shennan I and Woodworth PL. (1992) A comparison of late Holocene and twentieth-century sea-level trends from the UK and North Sea region. *Geophysical Journal International* 109: 96-105.

Simpson GL. (2012) Analogue methods. In: Birks HJB, Lotter AF, Juggins S, et al. (eds) *Data Handling and Numerical Techniques.* Springer, 495-522.

Spiegelhalter DJ, Best NG, Carlin BP, et al. (2002) Bayesian measures of model complexity and fit. *Journal of the Royal Statistical Society: Series B (Statistical Methodology)* 64: 583-639.

Stuiver M and Pearson GW. (1993) High precision bidecadal calibration of the radiocarbon timescale, AD 1950-500 BC and 2500-6000BC. *Radiocarbon* 35: 1-23.

Talke S and Jay DA. (2013) Nineteenth century North American and Pacific tidal data: lost or just forgotten? *Journal of Coastal Research* 29: 118-127.
Tanner BR, Uhle ME, Kelley JT, et al. (2007) C_3/C_4 variations in salt-marsh sediments: An application of compound specific isotopic analysis of lipid biomarkers to late Holocene paleoenvironmental research. *Organic Geochemistry* 38: 474-484.
Traverse A. (2007) *Paleopalynology*: Springer.
van de Plassche O. (1991) Late Holocene sea-level fluctuations on the shore of Connecticut inferred from transgressive and regressive overlap boundaries in salt-marsh deposits. *Journal of Coastal Research* 11: 159-179.
van de Plassche O, van der Borg K and de Jong AFM. (1998) Sea level-climate correlation during the past 1400 yr. *Geology* 26: 319-322.
Vane CH, Chenery SR, Harrison I, et al. (2011) Chemical signatures of the Anthropocene in the Clyde estuary, UK: sediment-hosted Pb, 207/206Pb, total petroleum hydrocarbon, polyaromatic hydrocarbon and polychlorinated biphenyl pollution records. *Philosophical Transactions of the Royal Society A: Mathematical, Physical and Engineering Sciences* 369: 1085-1111.
Varekamp J, Thomas E and van de Plassche O. (1992) Relative sea-level rise and climate change over the last 1500 years. *Terra Nova* 4: 293-304.
Varekamp JC. (1991) Trace element geochemistry and pollution history of mudflat and marsh sediments from the Connecticut coastline. *Journal of Coastal Research*: 105-123.
Varekamp JC, Brink MRBt, Mecray EL, et al. (2000) Mercury in Long Island Sound sediments. *Journal of Coastal Research* 16: 613-626.
Varekamp JC, Mecray EL and Maccalous TZ. (2005) Once spilled, still found: metal contamination in Connecticut coastal wetlands and Long Island Sound sediment from historic industries. In: Whitelaw DM and Visgilio GR (eds) *America's Changing Coasts.* Cheltenham, UK: Edward Elgar Publishing, 122-147.
Waller M. (2015) Techniques and applications of plant macrofossil analysis in sea-level studies. In: Shennan I, Long AJ and Horton BP (eds) *Handbook of Sea-Level Research.* Wiley-Blackwell, 183-190.
Walraven N, van Os BJH, Klaver GT, et al. (1997) Trace element concentrations and stable lead isotopes in soils as tracers of lead pollution in Graft-De Rijp, the Netherlands. *Journal of Geochemical Exploration* 59: 47-58.
Walsh DC, Chillrud SN, Simpson HJ, et al. (2001) Refuse incinerator particulate emissions and combustion residues for New York City during the 20th century. *Environmental Science & Technology* 35: 2441-2447.
Watcham EP, Shennan I and Barlow NLM. (2013) Scale considerations in using diatoms as indicators of sea-level change: lessons from Alaska. *Journal of Quaternary Science* 28: 165-179.
Wong K-C. (1990) Sea level variability in Long Island Sound. *Estuaries* 13: 362-372.
Wong PP, Losada IJ, Gattuso JP, et al. (2014) Coastal systems and low-lying areas. In: Field CB, Barros VR, Dokken DJ, et al. (eds) *Climate Change 2014: Impacts, Adaptation, and Vulnerability. Part A: Global and Sectoral Aspects. Contribution of Working Group II to the Fifth Assessment Report of the Intergovernmental Panel of Climate Change.* Cambridge, United Kingdom and New York, NY, USA: Cambridge University Press, 361-409.
Woodworth PL, Teferle FN, Bingley RM, et al. (2009) Trends in UK mean sea level revisited. *Geophysical Journal International* 176: 19-30.
Wright AJ, Edwards RJ and van de Plassche O. (2011) Reassessing transfer-function performance in sea-level reconstruction based on benthic salt-marsh foraminifera from the Atlantic coast of NE North America. *Marine Micropaleontology* 81: 43-62.

Yang Z. (2008) VDatum for the Long Island Sound, Narragansett Bay, and New York Bight tidal datums, marine grids, and sea surface topography. Silver Spring, MD: U.S. Dept. of Commerce, National Oceanic and Atmospheric Administration, National Ocean Service, Office of Coast Survey, Coast Survey Development Laboratory.
Yin J and Goddard PB. (2013) Oceanic control of sea level rise patterns along the East coast of the United States. *Geophysical Research Letters* 40: 5514-5520.
Yin J, Schlesinger ME and Stouffer RJ. (2009) Model projections of rapid sea-level rise on the northeast coast of the United States. *Nature Geoscience* 2: 262-266.

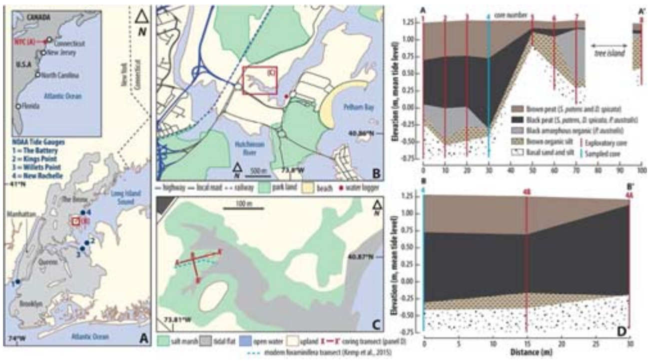

Figure 1: (A-C) Location of the Pelham Bay study site in The Bronx, New York City (NYC) and National Oceanic and Atmospheric Administration (NOAA) tide gauges (numbered blue circles in panel A). The inset in panel A shows the location of NYC and other proxy relative sea level reconstructions (Connecticut, New Jersey, North Carolina and Florida) on the U.S. Atlantic coast. (D) Sediment beneath the Pelham Bay salt marsh described from cores recovered along two transects (A-A’ and B-B’). Core number 4 (PBA-4) was selected for detailed analysis because it included the thickest sequence of peat and was representative of the stratigraphy at the site.

103x56mm (300 x 300 DPI)

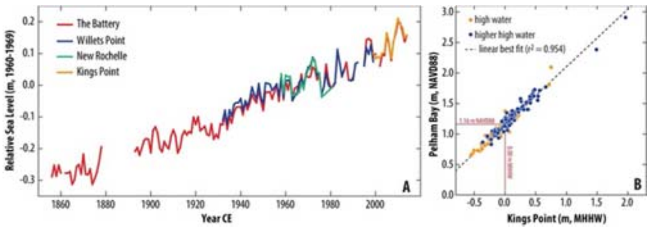

Figure 2: (A) Relative sea level measured by tide gauges in New York City. Annual data from The Battery, Willets Point and New Rochelle up to and including 2014 were downloaded from the Permanent Service for Mean Sea Level. The Battery is located at the southern tip of Manhattan and measures RSL in New York Harbor. The instruments at Willets Point and New Rochelle record RSL in Long Island Sound. Average RSL over the period 1960-1969 CE is the reference period for each tide gauge series. Monthly data (January 1999 to December 2014) for Kings Point were downloaded from the National Ocean and Atmospheric Administration and used to generate annual averages that in turn were referenced the RSL at The Battery. (B) Correlation between tides measured at the Pelham Bay field site using an automated water logger (relative to the North American Vertical Datum of 1988; NAVD88) and those measured by the NOAA operated tide gauge at Kings Point with respect to local mean higher high water (MHHW). At Willets Point MHHW lies 1.13 m above NAVD88.

64x22mm (300 x 300 DPI)

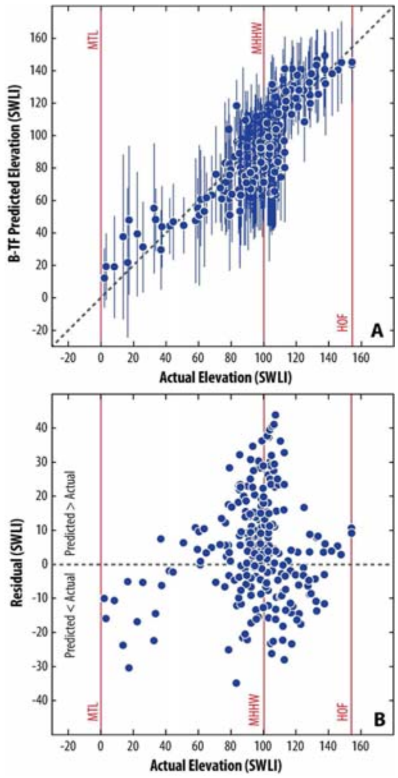

Figure 3: Assessment of the Bayesian transfer function's (B-TF) performance using cross validation. The modern training set was comprised of 254 samples from 12 salt marshes (including Pelham Bay) on the Long Island Sound coast of New York and Connecticut. (A) Comparison of actual elevations measured at the time of sample collection and predicted by the B-TF with 95% credible intervals. Dashed line represents parity between actual and predicted elevations. (B) Difference between actual and mean predicted elevations. MTL = mean tide level, MHHW = mean higher high water, HOF = highest occurrence of foraminifera in the modern training set, SWLI = standardized water level index.

146x290mm (300 x 300 DPI)

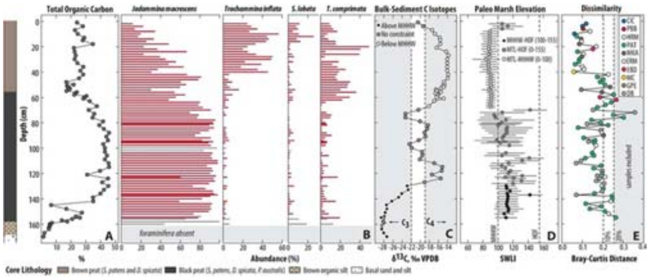

Figure 4: Sea-level indicators and paleomarsh elevation (PME) reconstructions from PBA-4. (A) Total organic carbon measured on bulk-sediment samples. (B) Relative abundance of the four most common species of foraminifera. For consistency with the modern training set, counts of Trochammina inflata and Siphotrochammina lobata were combined prior to analysis. Samples represented by grey bars had counts of fewer than 50 foraminifera and were excluded from the final relative sea level reconstruction. (C) Measurements of δ13C in bulk sediment samples relative to the Vienna Pee Dee Belemnite (VPDB) standard. Shaded areas denote values associated with environments dominated by C4 and C3 plant species. Symbol shading denotes the prior constraint placed on PME in the Bayesian transfer function based on the modern distribution of C4 and C3 plant communities on and around salt marshes in New Jersey, USA. (D) Paleomarsh elevation (mean with 95% credible interval) estimated using the Bayesian transfer function including the prior constraint provided by bulk sediment δ13C measurements. Symbol shading denotes the prior placed on each sample based on bulk-sediment δ13C measurements. SWLI = standardized water level index, HOF = highest occurrence of foraminifera, MHHW = mean higher high water. (E) Dissimilarity between core samples and their closest modern analogue in the modern training set measured using the Bray Curtis metric. Dashed vertical lines represent percentiles of dissimilarity measured for all possible pairs of modern samples. Core samples exceeding the 20% threshold were excluded from the reconstruction (grey shaded area). The 10% threshold is shown for comparison. Symbol colors denote the site that provided the closest modern analogue. CIC = Canfield Island Cove, PBB = Pelham Bay, HRM = Hammock River Marsh, PAT = Pattagansett, MKA = Menunketesuk, ERM = East River Marsh, EBD = East Branford, MC = Marsh Conservancy, GPE= Gulf Pond East, DB = Double Beach.

83x35mm (300 x 300 DPI)

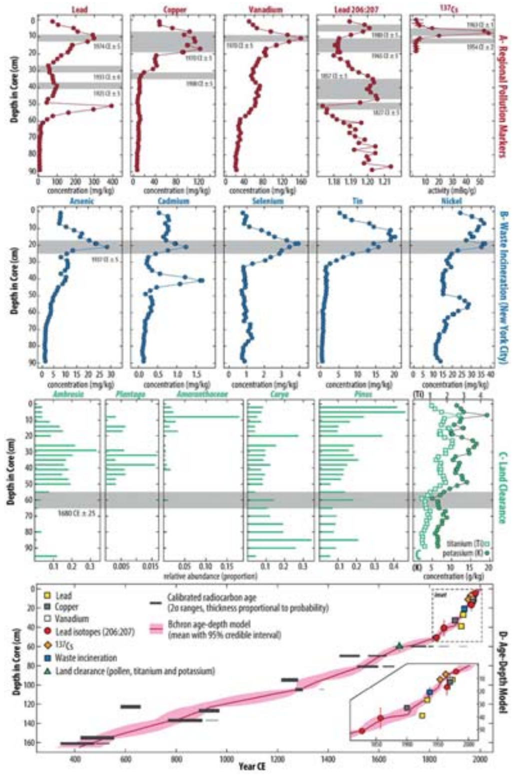

Figure 5: Chronology for PBA-4. Measurement uncertainties are smaller than symbols. Shaded envelopes represent the depth (with uncertainty) of each chronohorizon. Assigned ages with uncertainty are listed. (A) Elemental and isotopic profiles used to identify regional-scale pollution markers. (B) Suite of elemental profiles used to identify a local-scale pollution marker caused by incineration of domestic waste at sites throughout New York City in the early 20th century. (C) Recognition of a land-use marker horizon associated with clearance by European settlers from pollen profiles and the down core concentration of titanium and potassium. (D) Bchron age-depth model developed for PBA-4 (mean and 95% credible interval). Calibrated (2σ) radiocarbon ages are represented by grey bars thicknesses that are proportional to their probability. Inset shows last ~200 years in more detail.

228x348mm (300 x 300 DPI)

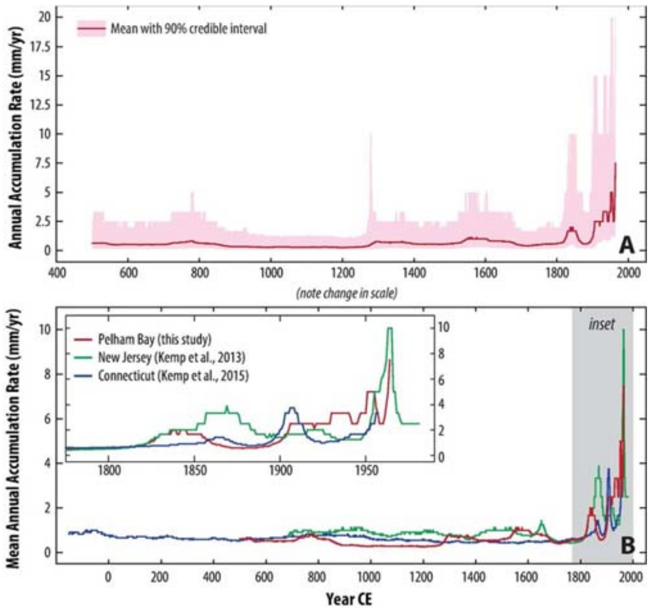

Figure 6: (A) Annual sedimentation rates for core PBA-4 estimated from the suite of chronologies generated by the Bchron age-depth model. Results are the mean (solid line) and 90% credible interval (5th to 95th percentiles; shaded envelope). (B) Comparison of late Holocene annual sedimentation rates from salt marshes in Connecticut, New York City and southern New Jersey. Sedimentation rates were estimated by applying the same approach to each dataset. For clarity of presentation only mean estimates are presented and details of sedimentation rates during the past ~250 years are shown in detail in the inset panel.

82x77mm (300 x 300 DPI)

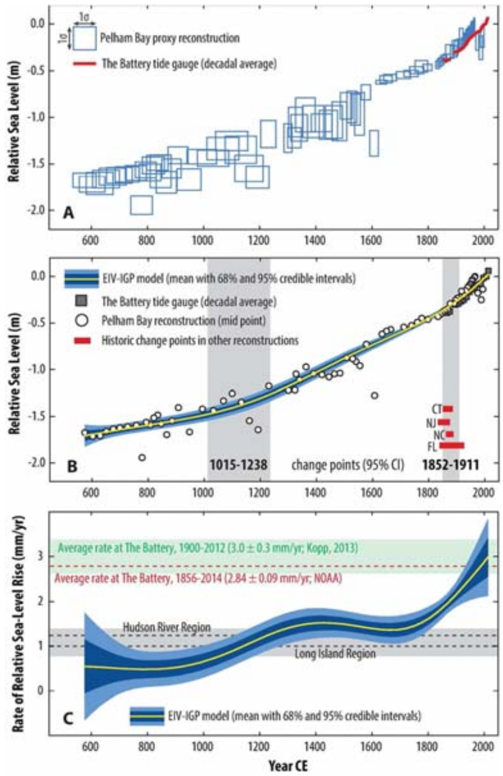

Figure 7: Relative sea level (RSL) reconstruction from Pelham Bay in New York City. (A) Proxy reconstructions are represented by boxes that encompass vertical and chronological uncertainties. Only 1σ uncertainties are shown for clarity, but subsequent analysis used the 2σ uncertainties. Annual RSL measurements from The Battery tide gauge were reduced to decadal averages (red line) and combined with the salt-marsh reconstruction from PBA-4 to provide a proxy and instrumental record of RSL change in New York City. (B) Results from the Errors-in-Variables Integrated Gaussian Process (EIV-IGP) model displayed as a mean with shading denoting the 68% and 95% credible intervals. For clarity of presentation reconstructions are represented by their mid points only. Vertical shaded regions show the timing of significant change points at 1015-1238 CE and 1852-1911 CE (95% credible ranges). Red bars show timing of historic change points identified in proxy RSL reconstructions from Connecticut (CT), New Jersey (NJ), North Carolina (NC) and Florida (FL) and reported by Kemp et al. (2015). (C) Rate of RSL change estimated by the EIV-IGP model presented as a mean with shaded 68% and 95% credible intervals. Positive values refer to RSL rise. The green shaded envelope marks the average rate of RSL rise measured by The Battery

tide gauge from 1900-2012 and reported by Kopp (2013), while the dashed red line marks the average linear rate of rise reported by the National Ocean and Atmospheric Administration (NOAA). Dashed grey lines (mean) and shaded grey area (uncertainty) represent the regional background rates of late Holocene RSL rise estimated by Engelhart and Horton (2012) for the Hudson River (1.25 ± 0.1 mm/yr) and Long Island (1.0 ± 0.3 mm/yr) regions and attributed primarily to ongoing glacio-isostatic adjustment.

137x214mm (300 x 300 DPI)

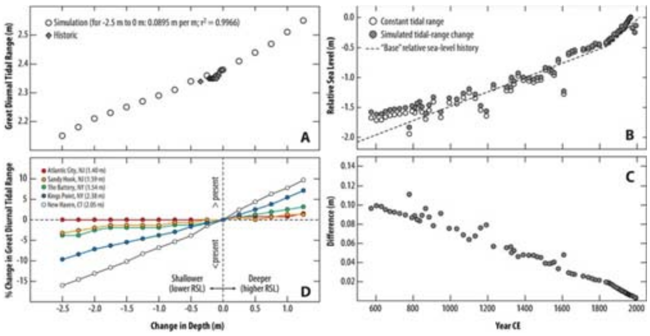

Figure 8: (A) Great diurnal tidal range (mean lower low water to mean higher high water) simulated for Kings Point using the Coastal Ocean model (open circles) with sea level varying from -2.5 m (shallower depths than present) to + 1.25 m (deeper than present). Historic measurements from the Willets Point tide gauge (filled diamonds) are shown for comparison, where measured relative sea level (RSL) change is assumed to correspond to a change in depth. (B) Effect of tidal-range change on the Pelham Bay RSL. The original RSL reconstruction assumes a constant tidal range during the past 1500 years (open circles). This reconstruction was adjusted for non-stationary tides (filled circles) by using an assumed RSL history (dashed line) in which the pre-1850 trend is driven solely by glacio-isostatic adjustment at 1.2 mm/yr and the post-1850 trend is provided by RSL measurements at the Battery in New York City. A paleo tidal range was estimated for each year in the "base" RSL history using the tidal simulations for Kings Point under the assumption that RSL change caused a corresponding depth change in Long Island Sound. (C) Difference in RSL between the original reconstruction and the one conservatively adjusted for possible tidal range change. (D) Percentage change in great diurnal tidal range (negative values indicate a smaller tidal range than present) simulated to occur at five tide-gauge locations when water depth is varied by -2.5 to + 1.25 m. The current range at each location is provided in the legend.

90x46mm (300 x 300 DPI)

Depth (cm)	Elevation (m, MTL)	BP	Hs	JM	TiSL
2	1.16	0	6	13	41
4	1.14	6	4	25	41
6	1.12	0	8	14	46
8	1.1	0	10	35	32
10	1.08	0	3	20	69
12	1.06	0	9	17	71
14	1.04	0	5	35	58
16	1.02	0	4	27	59
18	1	0	1	50	36
20	0.98	0	0	23	26
22	0.96	0	0	37	22
24	0.94	4	0	69	26
26	0.92	0	0	23	38
28	0.9	0	1	40	57
30	0.88	0	0	45	49
32	0.86	0	0	58	28
34	0.84	0	0	50	40
36	0.82	0	0	67	20
38	0.8	0	0	38	38
40	0.78	0	0	33	54
42	0.76	0	0	68	6
44	0.74	0	0	82	2
46	0.72	0	0	80	5
48	0.7	0	0	61	10
50	0.68	0	0	69	7
52	0.66	1	0	62	7
54	0.64	0	2	30	23
56	0.62	0	0	54	5
58	0.6	1	1	70	11
60	0.58	0	2	58	8
64	0.54	0	0	83	3
66	0.52	0	0	80	2
68	0.5	0	0	87	5
70	0.48	0	0	91	0
74	0.44	0	0	81	3
78	0.4	0	0	103	1
80	0.38	0	1	94	0
81	0.37	0	0	94	0

123	-0.05	1	1	60	7
124	-0.06	0	3	95	0
126	-0.08	3	0	96	0
128	-0.1	0	0	90	0
130	-0.12	0	3	75	10
132	-0.14	0	0	88	3
134	-0.16	0	1	95	0
136	-0.18	0	0	96	1
137	-0.19	0	0	98	0
138	-0.2	0	1	95	1
140	-0.22	0	1	86	2
142	-0.24	0	6	59	10

AI	MP	Interpretation	SWLI Prediction	
0	2	Intermediate	105.46	
0	0	Intermediate	113.06	
0	2	Intermediate	105.57	
0	5	Below MHHW	89.49	
0	1	Below MHHW	88.65	
0	0	Below MHHW	88.92	
0	0	Below MHHW	88.65	
0	0	Below MHHW	89.48	
0	0	Below MHHW	88.32	
0	2	Below MHHW	88.17	
0	0	Below MHHW	87.88	
0	0	Below MHHW	89.77	
0	0	Below MHHW	87.20	
0	0	Below MHHW	89.45	
0	0	Below MHHW	84.33	
0	0	Below MHHW	88.02	
0	0	Below MHHW	87.14	
0	0	Below MHHW	87.43	
0	1	Below MHHW	88.65	
0	0	Below MHHW	87.12	
0	6	Below MHHW	90.52	
0	0	Below MHHW	90.12	
0	0	Below MHHW	90.43	
0	0	Below MHHW	90.29	
0	0	Below MHHW	90.28	
0	5	Below MHHW	91.11	
0	4	Below MHHW	88.51	
0	3	Below MHHW	90.35	
0	8	Below MHHW	91.54	
0	5	Below MHHW	91.30	
0	12	Below MHHW	90.12	
0	17	Below MHHW	89.92	
0	13	Below MHHW	90.86	
0	9	Intermediate	142.57	1
0	8	Intermediate	94.88	
0	2	Intermediate	110.46	
0	0	Intermediate	105.14	
0	0	Intermediate	101.91	

0	1	Intermediate	110.09
0	1	Intermediate	120.77
0	0	Intermediate	131.17
2	9	Intermediate	119.93
0	4	Above MHHW	110.96
0	7	Above MHHW	111.66
0	3	Above MHHW	116.07
0	2	Above MHHW	112.22
0	2	Above MHHW	142.29
0	2	Above MHHW	113.21
0	9	Above MHHW	112.87
0	8	Above MHHW	112.22

RSL Error (m, 2σ)	AD2.5	AD10	AD50
0.220	2006	2003	1994
0.249	2000	1995	1986
0.195	1985	1980	1973
0.118	1968	1966	1965
0.153	1966	1965	1963
0.126	1960	1959	1956
0.112	1958	1957	1954
0.108	1957	1955	1952
0.128	1955	1953	1949
0.117	1952	1949	1943
0.125	1947	1944	1938
0.118	1943	1940	1935
0.118	1940	1937	1932
0.105	1935	1932	1925
0.224	1929.775	1926	1919
0.126	1923	1920	1912
0.131	1918	1914	1907
0.152	1916	1913	1905
0.119	1915	1911	1902
0.143	1905.775	1899	1874
0.073	1893	1882	1860
0.076	1878	1867	1852
0.079	1866	1857	1845
0.084	1857	1849	1838
0.081	1847	1840	1831
0.070	1830	1826	1813
0.124	1820	1813	1789
0.075	1810	1798	1766
0.068	1790	1777	1744
0.073	1762	1748	1704
0.072	1710.775	1692	1659
0.076	1694	1673	1644
0.039	1673	1654	1629
0.277	1637.775	1627	1609
0.165	1611	1601	1580
0.459	1590	1578	1556
0.335	1575	1564	1543
0.341	1564	1551.1	1533

0.180	979	959	936
0.204	954	938	927
0.234	940	929	912
0.353	921	912	889
0.159	911	897	868
0.180	900	885	849
0.181	886	868	828.5
0.171	868	846	807
0.200	855	830	790
0.160	834	811	769
0.167	814	788.1	739
0.171	791	765	711

Depth (cm)	δ15N (‰)	δ13C (‰)	% N	% N	CN ratio
1	6.16	-20.50	1.60	24.04	15.02
4	5.79	-19.33	1.60	28.09	17.58
7	5.31	-17.38	1.16	22.70	19.58
10	5.00	-16.79	1.15	24.55	21.36
13	4.54	-15.71	1.07	29.03	27.18
15	2.70	-15.64	1.14	27.96	24.43
18	1.89	-15.60	1.21	34.81	28.84
21	3.59	-16.39	0.95	22.03	23.15
24	1.63	-14.26	1.03	22.57	22.00
27	0.79	-13.81	1.04	23.25	22.41
30	0.69	-14.05	1.10	22.47	20.45
33	-0.08	-14.04	1.15	24.32	21.22
36	-0.51	-14.08	1.29	28.34	21.95
39	-0.65	-14.05	1.16	26.41	22.85
42	-0.24	-13.86	1.18	28.31	24.02
45	-0.36	-13.95	1.10	25.49	23.18
48	-0.30	-14.78	0.89	16.95	18.97
50	-0.24	-14.66	1.06	21.87	20.72
51	-0.39	-15.01	1.05	17.38	16.51
52	-0.45	-14.81	0.98	18.06	18.44
53	-0.46	-15.46	1.10	19.37	17.66
54	0.01	-16.58	1.05	18.72	17.79
55	0.32	-16.41	1.03	17.02	16.61
56	-0.16	-15.47	1.30	24.01	18.48
57	0.58	-16.62	1.44	22.83	15.85
58	0.32	-16.08	1.25	22.26	17.84
59	0.03	-16.22	1.58	30.50	19.25
60	0.06	-16.34	1.54	29.13	18.92
61	0.01	-14.86	1.38	28.35	20.50
63	0.09	-16.93	1.83	32.60	17.83
67	-0.07	-18.12	2.03	37.45	18.43
70	0.04	-20.40	1.92	32.02	16.68
73	-0.17	-23.24	2.03	35.66	17.57
76	-0.28	-23.28	1.99	34.55	17.33
79	-0.79	-20.04	2.06	41.67	20.19
82	-0.36	-18.30	2.10	39.09	18.62
85	-0.33	-18.47	2.41	42.15	17.52
88	-0.45	-19.04	2.51	45.72	18.25
91	-0.40	-18.83	2.43	43.93	18.11
94	-0.30	-20.33	2.42	44.99	18.60
97	-0.31	-22.38	2.23	41.79	18.77
100	-0.68	-21.89	2.34	42.83	18.29
103	-0.87	-19.61	2.30	42.87	18.60
106	-0.95	-19.54	2.39	44.28	18.50
109	-1.20	-20.10	2.20	42.82	19.43
112	-1.12	-16.91	2.08	45.35	21.81

115	-0.93	-15.14	1.89	45.70	24.16
118	-0.55	-15.28	1.90	39.62	20.83
121	2.66	-17.42	1.49	30.94	20.71
124	-0.21	-15.48	1.89	45.03	23.87
127	-0.10	-19.04	2.02	41.06	20.34
130	-0.41	-22.87	1.98	45.18	22.87
133	-0.41	-22.65	2.08	42.16	20.23
136	-0.17	-24.06	2.13	39.90	18.73
139	0.64	-24.76	1.99	34.90	17.55
142	0.46	-26.25	2.10	35.03	16.67
145	0.37	-27.43	0.32	6.73	20.98
148	0.51	-27.34	0.82	16.98	20.78
151	0.10	-27.72	0.93	27.49	29.66
154	0.39	-27.91	0.83	23.24	27.87
155	0.77	-28.61	0.90	26.01	28.80
156	0.78	-27.98	0.86	20.90	24.43
157	1.17	-28.04	0.55	13.88	25.26
158	0.34	-28.25	0.62	17.53	28.35
159	0.93	-27.87	0.25	7.24	28.50
160	1.37	-28.18	0.23	5.79	25.63
161	2.14	-28.53	0.25	6.08	24.44
162	2.17	-28.46	0.24	5.63	23.93
163	2.11	-28.45	0.22	5.13	23.83
164	2.09	-28.50	0.22	5.25	23.93
167	3.63	-28.05	0.09	2.21	23.57
170	4.13	-27.36	0.07	1.52	21.53

Element	Li	Be	Na	Mg
Detection Level (mg/kg)	<0.8	<0.2	<45	<7
Depth (cm)	mg/kg	mg/kg	mg/kg	mg/kg
1	19.49	0.66	62058.47	14527.42
2				
3	22.34	1.15	58267.03	13628.87
4				
5	26.10	1.41	51534.73	11773.49
6				
7	50.32	1.82	38973.73	12129.70
8				
9	31.19	1.71	40564.61	9158.72
10				
11	29.41	1.19	39742.34	9429.88
12				
13	29.69	1.38	39769.84	8830.58
15	36.23	1.57	36048.49	9928.96
15	35.35	1.61	36749.83	9898.74
17	30.47	1.16	40642.63	8297.56
19	27.62	1.77	44825.27	9262.02
19	27.15	1.50	44176.50	9748.58
21	27.04	1.19	50000.36	11631.27
23	26.22	1.45	48114.82	10780.27
25	29.06	1.29	50844.72	10200.50
27	26.45	1.40	52529.95	9714.70
29	25.84	0.94	54340.76	10422.01
31	33.61	0.95	51271.53	10830.39
33	37.74	1.29	49365.64	10582.26
35	27.85	0.50	52471.31	10220.54
37	29.14	0.71	55074.77	10342.63
39	24.24	1.18	58759.38	10591.48
41	26.56	1.04	59151.61	10474.38
41	26.34	1.29	59922.88	10471.91
43	27.75	1.02	67971.17	10643.12
45	36.35	1.00	76513.59	11772.86
47	40.21	0.88	72516.98	11901.42
49	41.55	0.72	74762.79	13742.39
51	45.39	0.88	57901.13	11330.30
[illegible]	[illegible]	[illegible]	[illegible]	[illegible]

K	Ca	Ti	V	Cr	Mn
<23	<10	<0.6	<0.4	<0.3	<0.6
mg/kg	mg/kg	mg/kg	mg/kg	mg/kg	mg/kg
11357.77	6636.42	1088.13	48.74	51.73	260.70
12473.57	5925.09	1293.28	57.18	40.02	181.83
13145.81	5184.74	1684.75	65.07	55.14	191.33
19271.34	4999.52	2712.23	94.97	94.48	272.22
12490.20	3919.24	1852.56	130.70	59.44	152.05
12224.90	3964.74	1782.25	159.01	60.67	143.89
10667.85	3959.41	1666.23	133.92	53.62	123.93
13097.09	4480.78	2085.56	106.68	58.43	166.73
12976.00	4248.86	2120.62	106.79	58.74	167.01
9825.63	3906.05	1578.53	84.89	43.95	105.88
9949.34	5036.04	1561.91	81.14	43.03	116.59
10246.49	5528.63	1623.09	82.56	43.94	119.84
12724.46	6772.13	1874.59	84.47	47.07	167.52
15527.30	6544.13	2318.59	69.95	49.91	135.46
16490.68	6024.00	2320.75	66.61	47.88	117.83
15860.88	5428.57	2245.21	63.17	46.66	106.83
14420.97	5578.27	1918.68	57.04	42.57	101.74
14618.21	5502.72	1933.96	58.11	42.00	134.62
11046.65	5059.14	1486.23	53.39	33.99	118.55
10376.60	5197.61	1354.90	56.40	31.56	91.70
12088.24	5185.85	1640.44	62.62	36.25	86.51
11763.38	5453.96	1579.06	71.70	36.33	72.78
11245.16	5260.47	1553.01	68.88	36.22	78.53
11416.61	5398.79	1650.60	70.42	37.25	79.58
11022.64	5127.72	1608.74	64.71	37.96	69.70
12721.64	5431.67	1796.53	68.38	40.76	76.51
12897.82	5100.26	1835.74	62.07	39.40	77.28
14017.00	5556.31	1926.60	62.86	41.41	98.46
11511.08	5143.19	1594.48	60.96	37.32	105.62

Cu	Zn	Ga	As	Se	Rb	S			
<0.07	<0.3	<0.03	<0.08	<0.07	<0.05	<0			
mg/kg	mg/kg	mg/kg	mg/kg	mg/kg	mg/kg	mg/			
47.39	63.84	5.78	8.02	0.78	38.56	113			
48.05	85.03	6.25	7.94	0.97	43.01	106			
71.30	106.80	8.04	7.72	0.90	52.72	100			
102.94	116.97	13.96	7.42	0.85	89.15	105			
92.80	90.74	9.34	10.38	1.15	52.90	78.			
110.95	92.55	9.61	13.93	1.84	51.95	80.			
113.14	87.49	9.89	17.39	2.25	42.86	85.			
99.11	94.28	12.19	16.59	2.58	58.89	92.			
98.60	93.49	12.40	16.66	2.58	57.40	91.			
122.38	73.39	11.37	20.54	3.28	39.19	84.			
91.43	86.24	11.17	23.31	3.77	38.19	94.			
89.81	89.98	11.73	23.72	3.93	40.88	96.			
41.75	111.87	12.41	28.38	3.42	52.39	113			
39.30	67.68	13.86	13.37	2.98	63.94	118			
40.36	36.21	13.26	10.72	2.86	65.88	118			
42.43	26.87	11.69	8.14	2.36	63.38	111			
35.92	28.85	9.71	10.86	2.05	59.14	108			
19.24	38.34	9.37	11.20	1.33	61.23	103			
13.76	47.54	7.17	11.10	0.82	45.10	92.			
10.99	42.97	6.81	9.99	0.82	41.30	93.			
10.93	51.58	8.57	8.13	0.87	49.50	97.			
11.49	78.03	8.06	10.43	0.90	45.37	100			
10.77	110.64	7.68	10.02	0.90	44.98	97.			
11.00	110.93	7.91	9.88	0.85	44.73	95.			
11.23	84.50	8.06	8.88	0.93	43.07	96.			
8.75	56.99	8.77	7.02	0.92	50.04	102			
7.95	41.88	9.20	6.43	0.71	53.64	98.			
7.14	40.87	9.74	5.59	0.75	61.01	104			
8.91	70.73	7.92	4.73	0.85	52.21	94			
6.83	12.70	3.24	1.35	0.88	16.51	112.10	6.80	16.82	2.07

6.83	12.70	3.24	1.35	0.88	16.51	112.10	6.80	16.82	2.07

Mo	Ag	Cd	Sn	Sb	Cs	Ba			
<0.03	<0.09	<0.009	<0.04	<0.02	<0.03	<0.			
mg/kg	mg/kg	mg/kg	mg/kg	mg/kg	mg/kg	mg/			
4.89	0.26	0.54	5.19	1.15	1.71	125.			
5.42	0.22	0.77	6.60	0.84	2.00	139.			
7.50	0.48	0.79	8.51	0.79	2.52	175.			
6.14	0.74	0.70	13.31	0.88	4.16	303.			
9.31	0.60	0.77	14.49	1.94	2.61	184.			
10.47	0.43	0.77	19.05	4.36	2.52	177.			
10.60	0.51	0.73	18.60	2.46	2.11	153.			
14.44	0.44	0.65	19.28	2.68	2.72	213.			
14.23	0.44	0.66	20.29	3.08	2.75	206.			
18.03	0.44	0.72	19.08	2.86	2.07	147.			
11.74	0.21	0.97	14.46	2.11	2.01	142.			
11.89	0.21	0.95	14.49	2.14	2.05	148.			
5.86	0.14	1.24	15.76	1.65	2.58	177.			
4.59	0.18	0.77	12.96	1.47	3.06	238.			
4.75	0.19	0.45	8.71	1.29	2.87	257.			
4.71	0.14	0.26	6.16	1.10	2.77	249.			
4.69	0.20	0.23	4.33	1.03	2.46	215.			
4.26	0.05	0.22	2.53	0.76	2.71	216.			
5.57	0.04	0.27	1.51	0.81	2.05	154.			
5.96	0.02	0.35	1.35	0.87	1.89	140.			
6.86	0.02	0.56	1.69	0.87	2.23	171.			
8.89	0.07	1.21	1.42	1.19	2.00	159.			
9.43	0.00	1.61	1.53	1.27	1.87	149.			
9.38	0.05	1.66	1.65	1.24	1.90	149.			
9.49	0.04	1.08	1.49	1.15	1.96	142.			
7.98	0.03	0.47	1.62	0.95	2.30	169.			
5.94	0.07	0.31	1.53	0.64	2.55	174.			
6.10	0.05	0.18	1.50	0.62	2.82	193.			
12.65	0.02	0.32	1.30	0.53	2.56	162.			
5.63	0.01	0.13	0.48	0.12	0.63	72.43	9.46	16.68	2.35

5.63	0.01	0.13	0.48	0.12	0.63	72.43	9.46	16.68	2.35

Nd	Sm	Eu	Tb	Gd	Dy	Ho			
<0.04	<0.02	<0.005	<0.004	<0.004	<0.005	<0.0			
mg/kg	mg/kg	mg/kg	mg/kg	mg/kg	mg/kg	mg/			
11.40	2.27	0.45	0.26	1.80	1.47	0.2			
13.15	2.65	0.52	0.29	2.04	1.65	0.2			
17.78	3.53	0.65	0.38	2.75	2.17	0.4			
26.12	5.09	0.99	0.57	4.04	3.14	0.5			
17.81	3.51	0.72	0.41	2.93	2.39	0.4			
17.69	3.54	0.70	0.39	2.85	2.33	0.4			
16.10	3.28	0.63	0.38	2.72	2.23	0.4			
19.83	3.83	0.81	0.47	3.24	2.64	0.4			
19.38	3.77	0.78	0.44	3.12	2.65	0.4			
14.78	3.02	0.60	0.34	2.45	2.08	0.3			
14.96	3.05	0.61	0.38	2.60	2.16	0.3			
16.18	3.05	0.65	0.36	2.63	2.23	0.3			
16.92	3.45	0.66	0.39	2.91	2.27	0.4			
19.42	3.70	0.76	0.42	3.00	2.37	0.4			
18.73	3.78	0.73	0.39	2.90	2.36	0.4			
17.57	3.44	0.74	0.36	2.59	2.15	0.3			
16.87	3.62	0.69	0.38	2.65	2.11	0.3			
19.54	3.92	0.75	0.42	2.94	2.37	0.4			
18.38	3.65	0.71	0.43	3.02	2.57	0.4			
17.47	3.63	0.72	0.44	2.89	2.47	0.4			
17.83	3.75	0.71	0.42	2.96	2.49	0.4			
17.00	3.43	0.71	0.41	2.88	2.37	0.4			
12.59	2.45	0.49	0.31	2.23	1.88	0.35	1.01	0.14	0.89
11.19	2.29	0.47	0.27	1.97	1.64	0.30	0.90	0.12	0.77
10.83	2.13	0.43	0.25	1.78	1.53	0.28	0.82	0.11	0.71
10.06	1.99	0.38	0.23	1.58	1.38	0.26	0.75	0.10	0.64
8.76	1.74	0.31	0.20	1.44	1.23	0.23	0.64	0.09	0.56
7.97	1.50	0.30	0.18	1.28	1.02	0.20	0.56	0.08	0.54
5.78	1.15	0.23	0.14	0.97	0.85	0.16	0.47	0.07	0.44
6.70	1.28	0.27	0.15	1.08	0.91	0.16	0.47	0.07	0.45
6.59	1.19	0.24	0.14	1.05	0.80	0.17	0.50	0.07	0.41
7.36	1.41	0.24	0.15	1.18	0.97	0.18	0.52	0.07	0.45
9.40	1.72	0.36	0.22	1.56	1.33	0.25	0.73	0.10	0.64

12.59	2.45	0.49	0.31	2.23	1.88	0.35	1.01	0.14	0.89
11.19	2.29	0.47	0.27	1.97	1.64	0.30	0.90	0.12	0.77
10.83	2.13	0.43	0.25	1.78	1.53	0.28	0.82	0.11	0.71
10.06	1.99	0.38	0.23	1.58	1.38	0.26	0.75	0.10	0.64
8.76	1.74	0.31	0.20	1.44	1.23	0.23	0.64	0.09	0.56
7.97	1.50	0.30	0.18	1.28	1.02	0.20	0.56	0.08	0.54
5.78	1.15	0.23	0.14	0.97	0.85	0.16	0.47	0.07	0.44
6.70	1.28	0.27	0.15	1.08	0.91	0.16	0.47	0.07	0.45
6.59	1.19	0.24	0.14	1.05	0.80	0.17	0.50	0.07	0.41
7.36	1.41	0.24	0.15	1.18	0.97	0.18	0.52	0.07	0.45
9.40	1.72	0.36	0.22	1.56	1.33	0.25	0.73	0.10	0.64

Lu	Hf	Ta	W	Tl	Pb	Bi			
<0.003	<0.02	<0.02	<0.002	<0.07	<0.05	<0.00			
mg/kg	mg/kg	mg/kg	mg/kg	mg/kg	mg/kg	mg/k			
0.09	0.55	0.25	1.21	0.23	74.94	0.38			
0.11	0.64	0.30	1.43	0.27	105.05	0.43			
0.13	0.79	0.38	2.12	0.34	188.26	0.54			
0.20	1.37	0.61	2.64	0.51	209.69	0.97			
0.17	0.87	0.41	3.19	0.41	291.42	0.81			
0.16	0.92	0.39	4.24	0.46	298.12	0.99			
0.14	0.76	0.36	3.77	0.48	263.37	0.71			
0.18	1.04	0.44	2.73	0.51	181.58	0.81			
0.18	1.05	0.44	3.04	0.49	180.82	0.80			
0.16	0.85	0.35	1.60	0.45	169.90	1.00			
0.13	0.84	0.33	1.74	0.41	157.68	0.83			
0.16	0.87	0.33	1.78	0.43	157.99	0.84			
0.15	0.88	0.39	2.17	0.42	121.37	0.74			
0.15	1.10	0.53	2.20	0.42	100.57	1.01			
0.16	1.18	0.54	1.92	0.37	79.89	0.69			
0.15	1.17	0.51	1.50	0.34	51.97	0.45			
0.15	0.99	0.43	1.12	0.29	58.24	0.31			
0.16	1.05	0.44	0.79	0.31	58.54	0.18			
0.15	0.78	0.33	0.49	0.24	74.33	0.16			
0.17	0.70	0.30	0.46	0.22	76.78	0.15			
0.14	0.86	0.37	0.60	0.28	80.70	0.13			
0.16	0.84	0.35	0.62	0.28	98.22	0.17			
0.13	0.49	0.19	0.32	0.13	8.33	0.03	2.81	9.57	1.193
0.11	0.49	0.24	0.35	0.18	6.44	0.03	3.05	8.27	1.198
0.11	0.48	0.20	0.35	0.12	5.09	0.02	2.75	8.14	1.195
0.09	0.46	0.19	0.32	0.15	4.50	0.04	2.74	7.86	1.205
0.07	0.40	0.17	0.25	0.12	6.16	0.04	2.27	6.28	1.192
0.07	0.37	0.14	0.20	0.14	4.26	0.04	1.89	5.13	1.205
0.06	0.26	0.10	0.16	0.07	3.82	0.04	1.37	4.18	1.200
0.07	0.31	0.13	0.19	0.08	4.71	0.04	1.69	4.29	1.201
0.05	0.29	0.12	0.18	0.08	4.75	0.04	1.56	4.42	1.198
0.06	0.30	0.12	0.18	0.09	6.04	0.04	1.68	4.54	1.214
0.09	0.51	0.14	0.24	0.14	7.01	0.05	2.06	5.37	1.203

0.13	0.49	0.19	0.32	0.13	8.33	0.03	2.81	9.57	1.193
0.11	0.49	0.24	0.35	0.18	6.44	0.03	3.05	8.27	1.198
0.11	0.48	0.20	0.35	0.12	5.09	0.02	2.75	8.14	1.195
0.09	0.46	0.19	0.32	0.15	4.50	0.04	2.74	7.86	1.205
0.07	0.40	0.17	0.25	0.12	6.16	0.04	2.27	6.28	1.192
0.07	0.37	0.14	0.20	0.14	4.26	0.04	1.89	5.13	1.205
0.06	0.26	0.10	0.16	0.07	3.82	0.04	1.37	4.18	1.200
0.07	0.31	0.13	0.19	0.08	4.71	0.04	1.69	4.29	1.201
0.05	0.29	0.12	0.18	0.08	4.75	0.04	1.56	4.42	1.198
0.06	0.30	0.12	0.18	0.09	6.04	0.04	1.68	4.54	1.214
0.09	0.51	0.14	0.24	0.14	7.01	0.05	2.06	5.37	1.203

137Cs
mBq/g
2.50
3.60
5.08
14.40
52.40
55.72
19.43
5.19
3.06
2.14
2.25
2.74
2.45

Depth (cm)	Pinus	Quercus	Carya	Liquidamba	Myrica	Sal
2	125	30	24	1	1	3
5	151	20	24	0	1	1
8	76	48	16	0	1	0
11	54	85	24	1	2	0
14	32	66	12	1	1	0
1	35	69	14	3	1	1
20	109	5	88	0	0	0
26	63	34	52	0	1	0
29	53	39	32	0	0	0
32	66	52	34	2	4	0
35	67	67	27	1	3	0
38	47	47	38	1	1	0
41	43	48	24	2	1	0
44	40	55	29	0	1	0
47	36	51	25	1	1	0
50	18	81	25	3	3	0
55	42	89	12	0	3	1

Ambrosia	Asteraceae	TCT	Ericaceae	Cyperaceae	Typha	Fabaceae	olygonacea	P03	PC3
11	4	0	0	1	0	1	0	0	1
12	11	1	1	1	3	0	0	0	4
12	4	0	0	4	1	0	0	2	2
26	10	0	0	1	3	1	0	1	1
42	13	1	0	4	1	0	0	1	1
55	10	0	0	5	1	0	0	0	0
27	9	0	0	1	1	0	0	1	0
74	8	0	0	1	0	0	0	0	0
113	5	0	0	1	0	1	0	2	1
72	6	0	0	2	0	0	0	2	3
54	3	0	0	0	0	0	1	1	5
49	2	0	0	0	0	1	0	1	0
60	2	0	0	1	0	2	0	2	1
46	0	0	0	0	1	0	0	0	0
57	2	0	0	1	0	0	0	1	1
60	3	0	0	0	0	2	0	1	2
23	6	0	0	3	0	1	0	0	2
10	7	0	0	3	3	0	0	1	1
4	10	1	0	31	3	0	0	2	0
3	13	0	0	32	0	1	0	0	0
0	7	1	0	110	0	0	0	0	0
11	8	0	0	61	0	1	0	0	1
2	1	0	1	25	0	0	0	0	3
4	6	0	0	4	0	0	0	2	3
36	15	0	0	22	0	0	0	0	1

PC0	SC0	SA0	Osmunda	Crumpled	Betula	Ulm
0	2	9	1	0	6	0
2	1	9	2	2	1	0
1	1	1	2	4	11	0
1	2	3	1	3	14	5
4	0	6	1	1	6	5
1	0	2	0	0	12	9
0	0	9	4	0	1	4
0	0	1	1	0	9	3
2	0	0	0	2	14	2
3	0	0	0	3	8	1
1	0	3	1	2	11	4
1	0	0	0	0	12	0
2	0	0	0	0	6	0
0	0	0	0	0	9	2
0	0	2	1	0	7	1
2	0	0	1	0	8	1
1	0	6	0	0	11	3

Plantago	O/C	Rosaceae	Coylus	Vitis	iriodendro	rthenociss	podium(nat	fagus	Juglans
0	0	0	0	0	0	0	0	0	1
0	0	0	0	2	0	0	0	0	7
1	0	0	0	0	0	0	0	1	0
0	1	0	0	0	0	0	1	3	1
2	0	0	0	0	0	0	0	0	1
2	1	0	1	0	0	0	0	5	5
0	1	0	0	0	2	0	0	0	0
0	0	0	0	0	0	0	0	4	7
2	1	0	0	0	1	0	0	3	0
6	0	0	0	0	0	0	0	6	4
1	0	1	0	0	0	0	0	3	5
5	0	0	0	0	0	2	0	11	2
2	0	0	0	0	0	0	0	3	0
2	0	0	1	0	0	0	0	5	2
1	0	0	0	0	0	0	0	2	3
1	0	0	0	1	0	0	0	2	0
0	3	0	0	0	0	0	0	11	0
0	1	0	0	0	0	0	0	2	0
0	0	0	1	0	0	0	0	3	0
0	0	0	0	0	0	0	0	7	0
0	2	0	0	0	0	0	0	1	2
0	1	0	0	0	0	1	0	3	0
0	0	0	0	0	0	0	0	1	1
0	0	0	0	0	0	0	0	2	0
0	0	0	0	0	1	0	0	1	0

Picea	tilia	Artemesia	Solanaceae	IVA	Tsuga	Olaceae	Euphorb	abies	waltheria
12	0	0	0	29	12	2	1	0	0
12	0	0	0	26	10	0	0	0	0
7	1	2	0	11	7	0	1	0	0
5	0	0	1	21	4	0	2	0	0
2	0	0	0	11	1	0	0	0	0
8	0	0	0	6	2	0	0	2	1
12	0	0	0	2	2	0	0	0	0
3	0	0	0	0	16	0	0	0	0
10	0	0	0	0	22	0	0	0	0
7	0	0	0	1	19	0	0	0	0
5	0	0	0	1	9	0	0	0	0
9	0	0	0	0	16	0	0	0	0
3	0	0	0	0	12	0	0	0	0
2	0	0	0	0	13	0	1	0	0
3	0	0	0	2	10	0	0	1	0
3	0	0	2	0	4	0	0	0	0
1	0	0	0	1	4	0	0	0	0
11	0	0	0	1	16	0	0	0	0
5	0	0	0	0	9	0	0	0	0
3	0	0	0	1	19	0	0	0	0
7	0	0	0	1	13	0	0	0	0
0	0	0	0	4	7	0	0	0	0
4	0	0	0	0	3	0	0	0	0
3	0	0	0	0	3	0	0	0	0
1	0	0	0	0	4	0	0	0	0

Depth (cm)
Elevation (m, MTL)
BP
Hs
JM
TiSL
TC
MF
AM
Rs
Al
MP
Interpretation
SWLI Prediction
l95
u95
RSL (m)
RSL Error (m, 2σ)
AD2.5
AD10
AD50
AD90
AD97.5
Pelham Bay d13C
Pelham Bay Pollution
Pelham Bay Pollen

Measured depth in core
Sample elevation with respect to modern mean tide level at Pelham Bay
Balticammina pseudomacrescens
Haplophragmoides spp.
Jadammina macrescens
Trochammina inflata + *Siphotrochammina lobata*
Tiphotrocha comprimata
Miliammina fusca
Arrenoparella mexicana
Reophax spp.
Ammoastuta inepta
Miliammina petila
Prior information provided to Bayesian transfer function based on bulk-sediment δ13C values. Intermediate indicates no additio
Standardized water level index predicted by Bayesian transfer function
Lower limit of the 95% confidence interval predicted by the Bayesian transfer function
Upper limit of the 95% confidence interval predicted by the Bayesian transfer function
Relative sea level with respect to present
Relative sea level uncertainty
Sample age (years AD), 2.5% confidence level
Sample age (years AD), 10% confidence level
Sample age (years AD), 50% confidence level
Sample age (years AD), 90% confidence level
Sample age (years AD), 97.5% confidence level
Downcore measurements of bulk-sediment δ13C, δ15N, %N, %C and C:N
Downcore elemental and isotopic data
Downcore pollen counts (raw abundance)

nal prior